International Journal of Nanomedicine

Dovepress
open access to scientific and medical research

Open Access Full Text Article

REVIEW

In vivo Biodistribution and Clearance of Magnetic Iron Oxide Nanoparticles for Medical Applications

Julia Nowak-Jary, Beata Machnicka

University of Zielona Gora, Faculty of Biological Sciences, Department of Biotechnology, Zielona Gora, 65-516, Poland

Correspondence: Julia Nowak-Jary, Email J.Nowak-Jary@wnb.uz.zgora.pl

Abstract: Magnetic iron oxide nanoparticles (magnetite and maghemite) are intensively studied due to their broad potential applications in medical and biological sciences. Their unique properties, such as nanometric size, large specific surface area, and superparamagnetism, allow them to be used in targeted drug delivery and internal radiotherapy by targeting an external magnetic field. In addition, they are successfully used in magnetic resonance imaging (MRI), hyperthermia, and radiolabelling. The appropriate design of nanoparticles allows them to be delivered to the desired tissues and organs. The desired biodistribution of nanoparticles, eg, cancerous tumors, is increased using an external magnetic field. Thus, knowledge of the biodistribution of these nanoparticles is essential for medical applications. It allows for determining whether nanoparticles are captured by the desired organs or accumulated in other tissues, which may lead to potential toxicity. This review article presents the main organs where nanoparticles accumulate. The sites of their first uptake are usually the liver, spleen, and lymph nodes, but with the appropriate design of nanoparticles, they can also be accumulated in organs such as the lungs, heart, or brain. In addition, the review describes the factors affecting the biodistribution of nanoparticles, including their size, shape, surface charge, coating molecules, and route of administration. Modern techniques for determining nanoparticle accumulation sites and concentration in isolated tissues or the body in vivo are also presented.

Keywords: magnetic nanoparticles, iron oxide nanoparticles, biodistribution, biodegradation

Introduction

Magnetic nanoparticles/iron oxide nanoparticles (MNPs/IONPs) (magnetite Fe_3O_4 and maghemite γ-Fe_2O_3) have been under intensive investigation since they show great potential for biomedical applications, such as tumors imaging (MRI),[1–3] radiolabelling and internal radiotherapy,[4] hyperthermia,[5,6] gene therapy,[7] biomolecules separation[8,9] and drug delivery.[9,10] Drug delivery is a vast field of MNPs applications as they possess a relatively large surface that enables binding and carrying other compounds, which can be directed using an external magnetic field to specific places in the body.[11] Additionally, nanoparticles depending on their size, can penetrate almost all tissues. Importantly, drugs immobilized on MNPs usually gain more beneficial properties, such as better solubility in water[12] and higher cytotoxicity to cancer cells.[13,14]

The uniqueness of iron oxide nanoparticles lies in their ferromagnetic nature. They consist of areas of permanent magnetization (so-called magnetic domains), generating a magnetic field around them (like small magnets). Ferromagnets are ferromagnetic below the Curie temperature and paramagnetic above. Magnetization is changing the direction of magnetization in domains or the boundaries of domains. All elementary magnetic dipoles align with an external magnetic field at magnetic saturation. The external magnetic field can guide magnetite and maghemite nanoparticles to specific locations in the body.[15,16] In the case of magnetic-targeted drugs, such as anti-cancer drugs, this results in lower toxicity and lower doses. Ferromagnetism distinguishes MNPs from other types of nanoparticles used in medicine, such as gold (AuNPs), silver (AgNPs) nanoparticles, or polymer nanoparticles (PNPs).

Received: 20 April 2023
Accepted: 29 June 2023
Published: 26 July 2023

Graphical Abstract

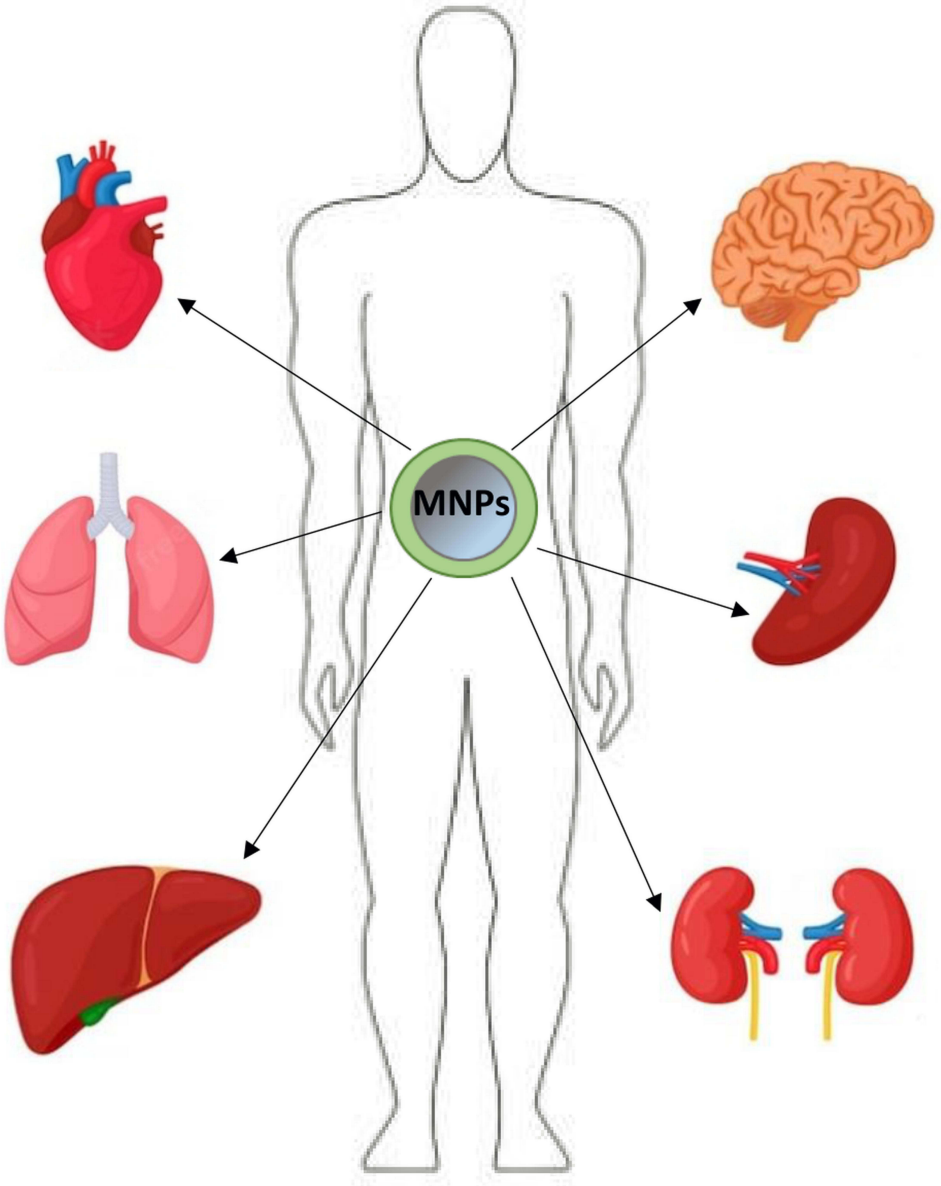

On the surface of AuNPs, electrons oscillate under the influence of light (surface plasmon resonance). AuNPs can scatter light intensely and are photostable, which makes these particles attractive imaging tools.[17] They are also used as contrast agents in computed tomography.[18] Among nanoparticles, AuNPs, and MNPs have also gained prominence as nanoradiopharmaceuticals for cancer imaging and therapy due to their biocompatibility, functionalization capabilities, and radiolabeling potential.[19–25] These targeted nanobrachytherapy approaches offer less invasiveness and improved radiation dose distribution compared to conventional treatments. Silver nanoparticles also show radiosensitizing properties.[26] Unfortunately, the main disadvantage of metallic nanoparticles is their non-biodegradability and toxicity. For example, the mice given 8 mg/kg AuNPs per body developed fatigue and a crooked spine, most of which died within three weeks.[27] In addition, Cho et al studied that PEGylated AuNPs (maximum dose 4.26 mg/kg) caused apoptosis of liver tissue.[28] An interesting type of nanoparticle in medical applications is also polymer nanoparticles (PNPs), such as nanospheres with a matrix structure, nanocapsules, dendrimers, and nanomicelles.[29–31] Some of them, similarly to

magnetic nanoparticles, enable drug release in a controlled and sustained manner and increase the solubility of lipophilic drugs.[31] Unfortunately, most PNPs have not been adequately tested regarding toxicology. Furthermore, there are difficulties in increasing the scale of their production, and the costs of producing some of them are very high.[31]

Magnetic iron oxide nanoparticles, unlike other metallic particles, are mainly biodegradable. The biodegradation mechanism of MNPs is believed to be analogous to ferritin metabolism, which is digested by lysosomal enzymes to release iron ions.[32] Many studies indicate that magnetic nanoparticles show low toxicity, causing only short-term, temporary changes, eg, oxidative stress, but do not contribute to permanent damage to organs.[33–40] Only extremely high doses (500 mg Fe/kg) caused pathological changes in the liver and spleen.[41]

Biodistribution of magnetic nanoparticles in the organism is an important parameter, the knowledge of which makes it possible to reduce the toxicity of nanostructures, which is a result of, inter alia, their undesirable distribution, as well as to increase the expected functionality of MNPs in a selected, targeted organ or tissues.[42] The parameter determines the amount and place of MNPs accumulation in various body organs during or after their application in vivo.[43] Biodistribution is closely related to the physicochemical properties of nanoparticles, such as size, coating molecules, and surface charge.[43,44]

The commonly used approach for administering MNPs is an intravenous injection, especially for their use as MRI contrast agents and in the case of clinical oncology.[43] The intravenously administered nanoparticles are selectively taken up by the liver and spleen, constituting the main pathway for removing MNPs from the body. Both organs form the mononuclear phagocytic system (MPS), also known as the reticuloendothelial system (RES). It should be noted that although MPS and RES nomenclatures are most often used interchangeably concerning macrophages, RES comprises only sinusoidal epithelial cells in the liver.[45] MPS consists of circulating monocytes in the blood and macrophages in various organs such as the liver, spleen, lymph nodes, bone marrow, lungs, and brain.[46] Among the specialized macrophages, there are, among others, Kupffer cells present in the sinusoidal capillaries of the liver, microglial cells found in the brain, as well as macrophages inhabiting secondary lymphatic organs, such as the spleen, and more specifically the red pulp and marginal zones of this organ.[46,47] By phagocytosis and engaging other macrophages from the bloodstream, macrophages cleanse the body of pathogens, damaged and old cells, and foreign bodies, including MNPs.[47,48] Although the liver and spleen are the main sites of nanoparticle uptake,[49] when injecting high doses of MNPs, their excess is accumulated in other tissues and organs such as lungs, heart, or adipose tissue.[50] It should be emphasized that the opsonization of nanoparticles precedes the uptake in the liver and spleen.[51,52] The opsonization process involves attaching specific proteins in the bloodstream to the surface of MNPs. These marking proteins are primarily immunoglobulins (IgA and IgM), complement components (C3, C4, C5),[53] and blood serum proteins (albumins, fibrinogen, fibronectin, C-reactive protein, type-I collagen).[54] Due to the protein labeling, the nanoparticles are recognized by macrophages.

The Main Organs and Tissues Involved in the Accumulation of Magnetic Nanoparticles

Liver

Blood from both the portal vein and hepatic artery mixes in the hepatic sinusoids. Sinusoidal capillaries, which are highly fenestrated with an average pore size of 100–180 nm, contain specialized macrophages called Kupffer cells (Figure 1).[55] Kupffer cells comprise the largest population of tissue macrophages in the organism and play a crucial role in the immune response efficiently phagocytizing pathogens entering from the bloodstream, including MNPs. Hepatocytes are separated from the sinusoids by a region called Disse space.[56] Ito cells in Disse space store fat-soluble vitamins. Kupffer cells quickly uptake large nanoparticles (> 100 nm) or agglomerates,[57] whereas smaller nanoparticles (< 100 nm) are captured in the Disse space. Hence, if they are provided with a suitable "shell", they can accumulate in hepatocytes.[58] Distribution in hepatocytes can be increased inter alia by attaching to nanoparticles of molecules with high affinity for these cells, such as linoleic acid[59] or by functionalization of the MNPs surface using antifouling molecules such as PEG[60] which reduce the degree of opsonization.

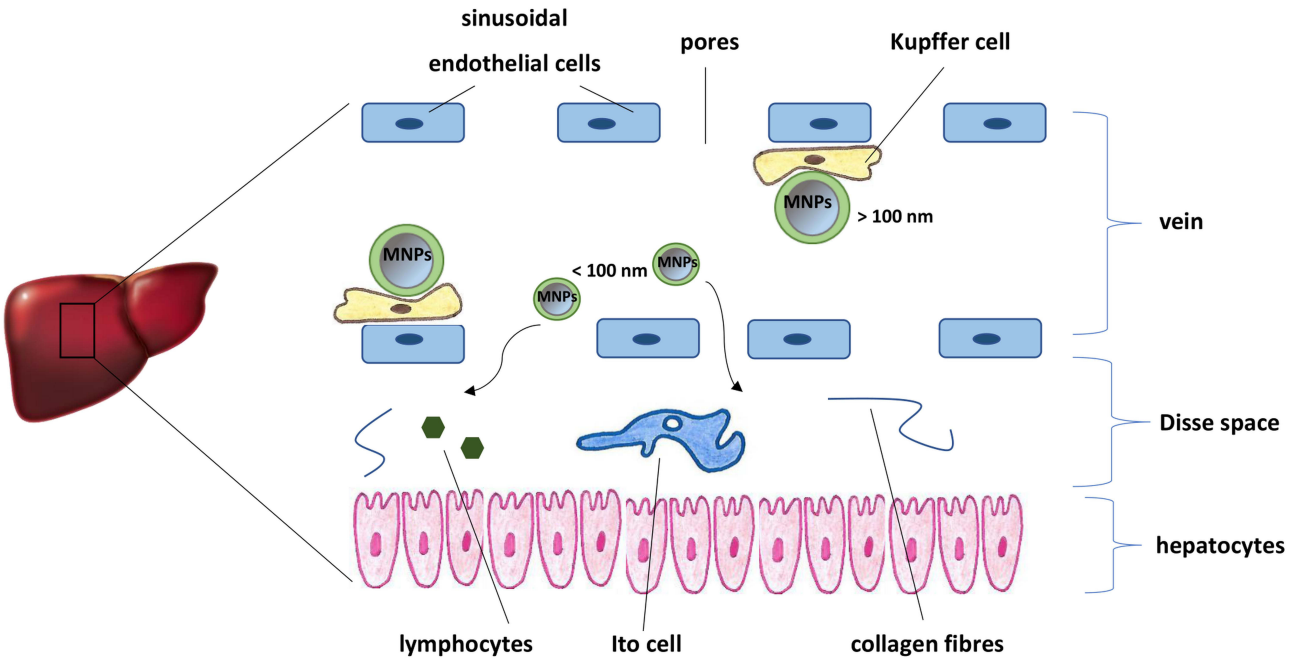

Figure 1 In the liver, Kupffer cells can quickly uptake large nanoparticles (> 100 nm), whereas smaller nanoparticles (< 100 nm) are captured in the Disse space from where, if suitably functionalized, they can also accumulate in hepatocytes.

Many reports in the literature indicate that the liver is the primary capture and biodistribution site for magnetic nanoparticles, both in the short and long term. A series of detailed studies in this field have confirmed it. For example, Tate et al[61] tested the biodistribution of two types of magnetite nanoparticles coated with hydroxyl-ethyl starch with an average hydrodynamic diameter of 110 nm and 20 nm in mice models. The results showed that the liver next to the spleen was the primary site of iron accumulation after 72 h for larger-sized nanoparticles (approx. 1.6 mg Fe/g tissue) (Figure 2A). Their level in this organ was still high even after 14 days after injection (Figure 2B). In contrast, image quantification of the heart, brain, and lung showed no significant difference in mean percent iron content.

Other studies have shown that polyacrylic-coated nanoparticles with an average diameter of approx. 10 nm after intravenous injection in mice models were also mainly accumulated in the liver.[33] The iron level in this organ 24 h after injection was about 2.5 mg/g of organ at a dose of 50 mg/kg body weight. This value was equivalent to approx. 6.5% liver weight/per total weight ratio, whereas in the case of the spleen, the ratio was around 0.41% spleen weight per total weight ratio. The high biodistribution of magnetic nanoparticles was also confirmed in the rabbit liver.[62] The authors used iron oxide nanoparticles covered with phosphated starch with a hydrodynamic diameter of 100–250 nm, which were intraarterially or intravenously injected. Shortly after application, the amount of the detected nanoparticles in the liver was 44% of the whole amount of the MNPs administered in the case of intraarterial injection and 73% in the case of intravenous injection.

Moreover, these values were not affected by the sizes of nanoparticles. Another study investigated the biodistribution of ultra-small superparamagnetic iron oxide nanoparticles used for MRI in BALB mice.[63] The nanoparticles were labeled with radioisotope ^{99m}Tc and administered via intravenous injection (the average diameter of ^{99m}Tc-MNPs was 41 nm). About 75% of injected doses were found in the spleen and liver at 15 min post-injection. While about 24% injected dose remained in the liver after 48 h post-injection, it was just about 3% in the spleen. Wang et al investigated the biodistribution of ^{111}In-radiolabeled PEGylated superparamagnetic iron oxide nanoparticles with a size range of 5–25 nm in the mouse.[64] The results showed that the liver exhibited the highest radioactivity concentrations (10 min, 30 min, 1 h, 2 h, and 24 h), followed by the spleen. After 24 h, radioactivity reached the value of 37% per gram of organ (for comparison – the radioactivity values after that time in the spleen and kidney were 21% and 8%, respectively). In summary, presented studies show that the liver is the initial filtration point where magnetic nanoparticles accumulate.

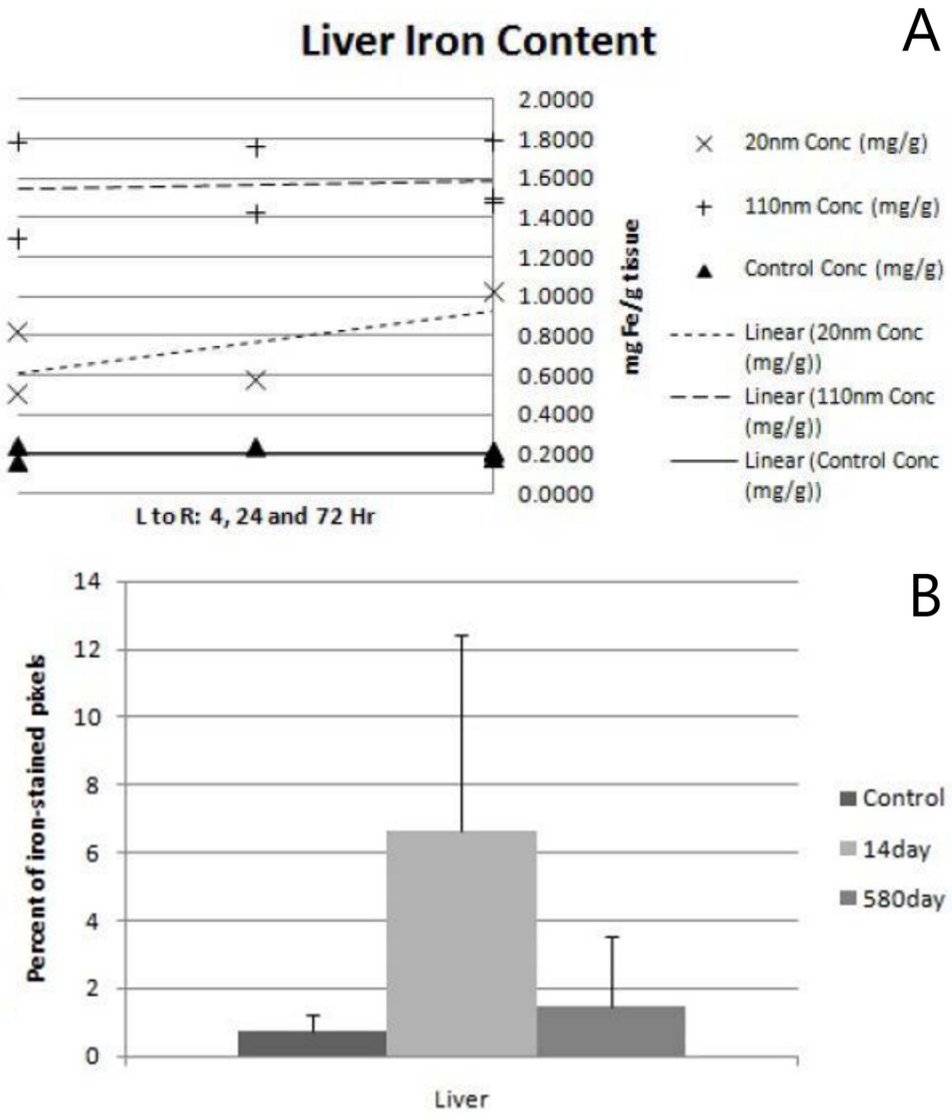

Figure 2 ICP-MS liver iron content after 72 hours (**A**) and after 14 days (concerns 110 nm-sized MNPs) (**B**). Percent of iron-stained pixels in liver tissue (iron-stained pixels were identified by calculating the Euclidian distance of each pixel to an average iron-stained RGB value given from a Prussian Blue iron-stained control slide). Used with permission of SPLE, from In Vivo Biodistribution of Iron Oxide Nanoparticles: An Overview. Energy Based Treat Tissue Assess, Tate JA, Petryk AA, Giustini AJ, Hoopes PJ. 2011; permission conveyed through Copyright Clearance, Inc.[61]

Because of the high accumulation in the liver, iron oxide nanoparticles have been successfully used as MRI T_2 contrast agents in this organ.[65,66] In particular, it is beneficial for detecting potential liver tumors as MNPs are taken up by Kupffer cells in healthy parts of the liver generating dark contrast in T_2-weighted MRI. In contrast, cancer cells not containing Kupffer cells appear as bright regions.[67] Xu et al have shown that glutathione-responsive hyaluronic acid-coated magnetic nanoparticles (H-MNPs) can be used for highly sensitive liver metastases (LMs) diagnosis.[68] The detection of small LMs is still challenging because of the subtle differences between normal liver tissue and small metastases. The authors demonstrated that H-MNPs greatly enhanced the signal of MRI in tumor metastases as a T_1 contrast agent. In contrast, they substantially decreased the signal of the liver as a T_2 contrast agent as they aggregated into clusters upon the high glutathione level in the liver.

Consequently, MRI contrasted by H-MNPs clearly distinguished metastatic tumors (bright) from surrounding liver tissues (dark). Moreover, there are reports that magnetic nanoparticles can be applied for liver fibrosis theranostics.[69] For example, Saraswathy et al tested citrate-coated magnetic nanoparticles with an average diameter of 12 nm and observed

an apparent dose-dependent contrast enhancement in a T_2-weighted in vivo MR imaging of liver fibrosis model in rodents.[70] On the other hand, due to such a significant capture of nanoparticles by the liver, their delivery to other tissues and target organs may be insufficient.[71] Thus, as there is the possibility of synthesizing nanoparticles of different sizes, morphology, and surface chemistry, there is a need for more extensive research into the type of interactions of magnetic nanoparticles with the liver to design nanoparticles according to therapeutic goals.

Lymphoid Organs: Spleen and Lymph Nodes

The spleen and lymph nodes are secondary lymphatic organs that function as biological filters protecting the body against microbes and cancerous cells.[72] They are also the site of the proliferation and maturation of T and B lymphocytes. The outer layer of the spleen is a compact connective tissue capsule, while its parenchyma consists of two types of interpenetrating tissues called white and red pulp (Figure 3A). Blood through the splenic artery first enters the white pulp and then, through smaller arterioles, reaches the red pulp, which constitutes 75% of the volume of the entire organ.[73] The spleen's primary immunological function is to remove pathogens and foreign particles (including MNPs) and to destroy old and senescent red blood cells (RBC) digested by phagocytic macrophages in the red pulp. The iron from RBC is removed and transported to be stored as ferritin.

Macrophage phagocytic pathogens, including magnetic nanoparticles, are found in the marginal zone of the spleen, which separates the red and white pulp. There is also a population of macrophages in the white pulp, performing functions similar to those in lymph nodes.[74] In red pulp, macrophages play the role of cleansing the blood of residual erythrocytes and are involved in iron recycling. On the other hand, there are reports that magnetic nanoparticles, although mainly phagocytosed by macrophages in the marginal zone, are also captured by macrophages in the red pulp of the spleen.[75,76]

Lymph nodes vary in size and shape and are found clustered at specific locations throughout the body. Each lymph node is divided into several regions: fibrous capsule, outer (nodular) cortex rich in B-cells, inner cortex (paracortex) rich in T-cells, and medulla – the central inner part of the node that contains large numbers of fixed phagocytic macrophages (Figure 3B).[72] MNPs can get into the lymph surrounding the tissues and then, through the lymphatic vessels, are directed to the lymph nodes, where they are trapped in a sinusoidal mesh containing macrophages.[77–79] The significant fraction of

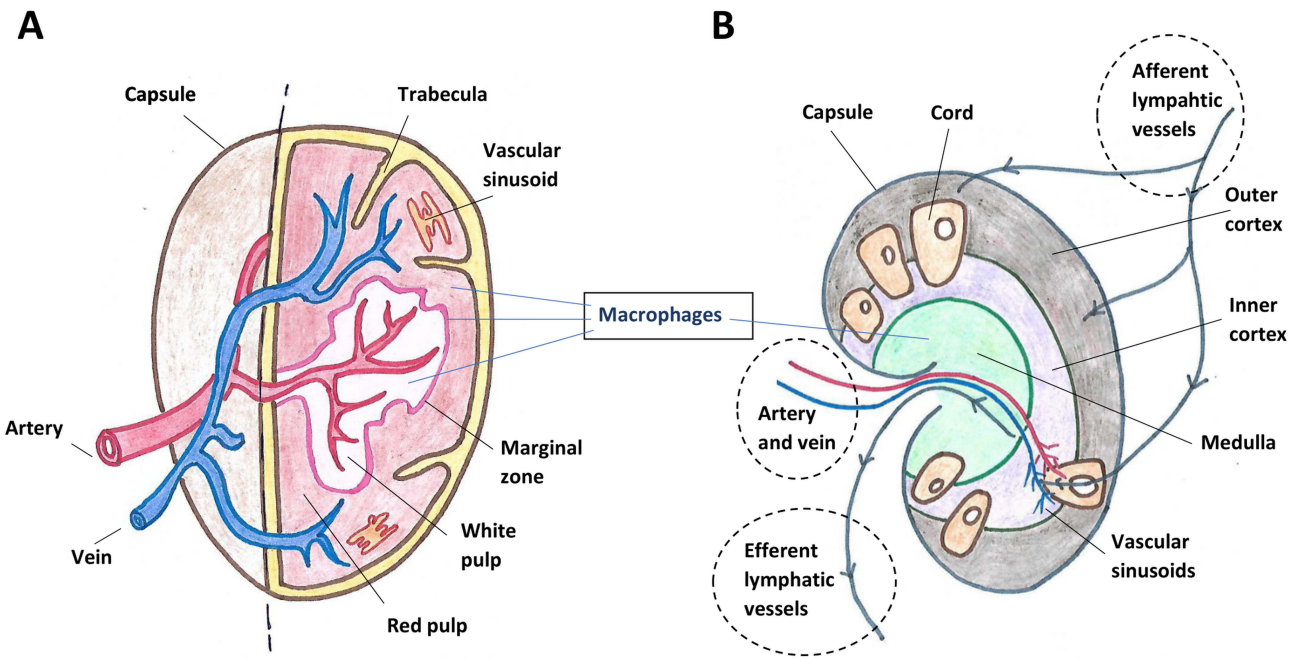

Figure 3 Schematic structure of spleen (**A**) and lymph node (**B**).

the intravenously injected MNPs is usually first captured by the liver and spleen. However, regional lymph nodes may be the initial filter point if magnetic nanoparticles are administered intramuscularly or subcutaneously.

A series of reports demonstrate a high accumulation of magnetic nanoparticles in the spleen. For example, about 10 nm-sized curcumin-coated MNPs administered intravenously in repeated doses in mice model reached a high level in the spleen 3 days after the final injection (about 110 µg Fe/dl; for comparison - this value in the case of the liver was about 60 µg Fe/dl).[34] In other studies, oleic acid-pluronic-coated MNPs were administered intravenously in rats. The Fe level was the highest in the spleen, reaching approximately 1200 µg/g of tissue after 21 days of injection.[35] The accumulation of these nanoparticles in the spleen was the highest compared to the other organs tested (Figure 4).

Kidneys and Non-Phagocytizing Clearance Pathway

The kidney, a bean-shaped organ, has a hilum, the passageway for the renal vessels and the ureter. The primary function of this organ is the filtration of fluids from the bloodstream, discarding the excess water and ions and eliminating nitrogenous waste, toxins, and drugs from the body. Each kidney contains over a million tiny structures called nephrons responsible for forming urine. Nephrons contain glomerular vessels that involve infiltration.

The intravenously injected MNPs enter the kidney with an artery in the renal hilum and reach glomeruli in nephrons. In glomeruli, cells called podocytes wrap around capillaries. If MNPs can get through the glomerular endothelium and

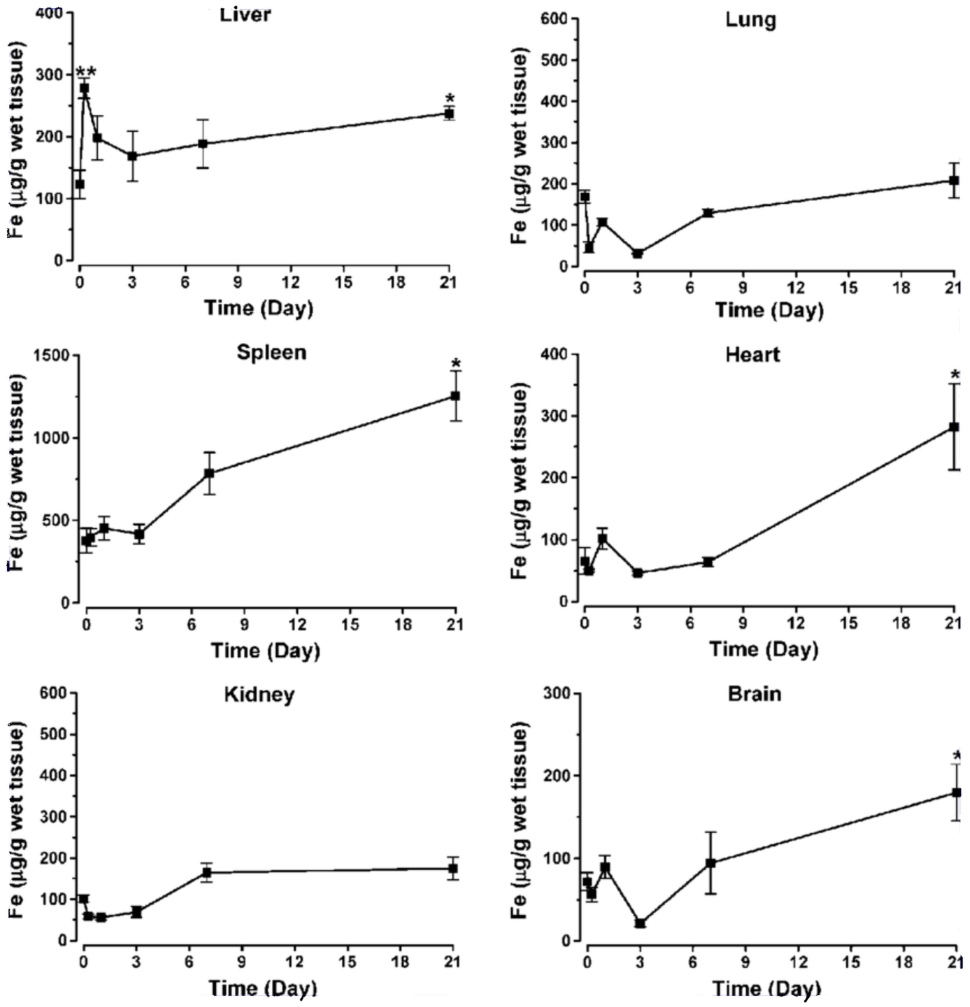

Figure 4 Changes in iron levels in different tissues following intravenous injection of MNPs. The injected dose of iron was 10 mg/kg in 100 µL of saline. Data presented as mean ± sem (n = 4). *p < 0.05 or **p < 0.005 vs saline. Reprinted with permission from Jain TK, Reddy MK, Morales MA, Leslie-Pelecky DL, Biodistribution, Clearance, and biocompatibility of iron oxide magnetic nanoparticles in rats. Mol Pharm. 2008;5(2):316–327. Copyright©2008, American Chemical Society.[35]

fenestrations between the podocytes, they are eventually extracted in urine via the ureter. This applies to nanoparticles smaller than 10–15 nm.[44,80]

Many studies have been performed showing renal clearance of small magnetic nanoparticles. For example, Kim et al developed iron oxide nanoparticle-based T_1 musculoskeletal contrast agents having an inverted core−shell structure of a dextran core and an iron oxide shell (i-MNPs) and a size of 3 nm.[81] One of the beneficial features of these nanoparticles is their compact hydrodynamic diameter, which is smaller than the renal filtration size limit. Intra-articularly injected i-MNPs were entirely excreted through renal clearance (Figure 5). According to the authors, it was the first successful demonstration of the renal clearance of intra-articularly injected nanomaterials.

Other studies showed the use of MNPs for the thermoablation of malignant kidney tumors in rabbits.[82] The nanoparticles' core size was 9–12 nm. In most cases, the applied ferrofluid was concentrated within the tumor mass. Additionally, a small portion of the ferrofluid was found in the renal pelvis or collecting duct. However, one should be careful when interpreting the results of the biodistribution of nanoparticles in the kidney, especially if that is the case with MNPs labeled with fluorophores. It is possible to locate the particles of the fluorophores themselves released from the nanoparticles as within the GBM (glomerular basement membrane), the nanoparticles can be disassembled by the numerous heparan sulfate molecules (Figure 6).[83] Once disassembled, the nanoparticle components can cross the remainder of the GBM and the podocyte filtration slits and enter the urinary space.

Furthermore, the fluorescent signal in the kidneys or MRI contrast enhancement in this area does not necessarily mean the uptake of MNPs by the glomeruli but only the result of the circulation of nanoparticles in the capillaries and arterioles of the renal cortex. The results obtained for PAMAM-dendrimer-coated MNPs with a core size of 10 nm and a huge hydrodynamic size of 242 nm may confirm the above.[84] The studies' authors demonstrated that kidneys were the

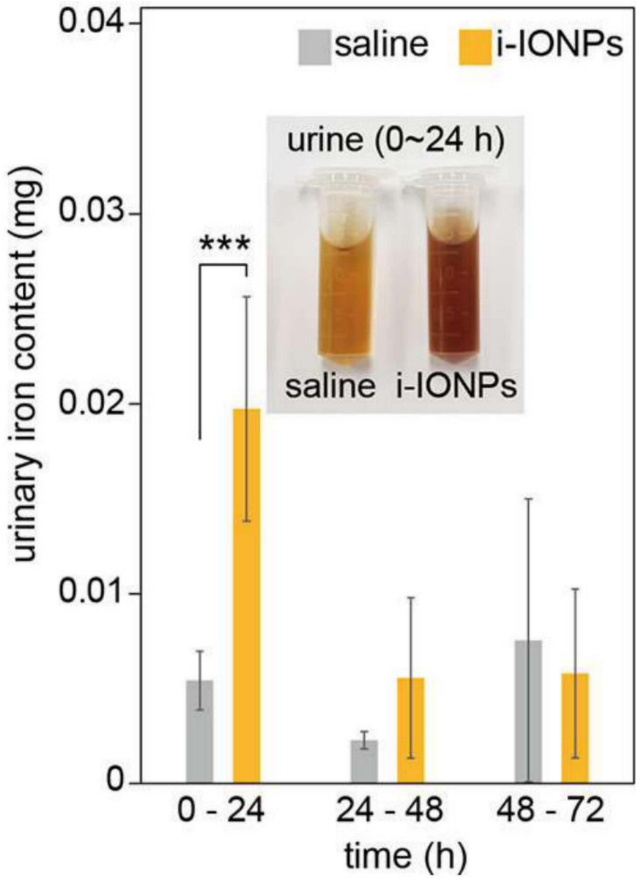

Figure 5 Renal excretion of intra-articular injected i–IONPs (i-MNPs): cumulative urinary iron content of male rats after intra-articular injection of i–IONPs (i-MNPs) and saline (inset: representative photos of urine samples of saline-injected (left) and i–IONPs-injected (right) rats. n = 5 biologically independent rats for each group. Error bars represent the standard deviation (***P < 0.001). Reprinted with permission from Wook KJ, Cheong J, Cheong H, et al. Iron oxide-coated dextran nanoparticles with efficient renal clearance for musculoskeletal magnetic resonance imaging. ACS Appl Nano Mater. 2021;4(12):12943–12948. Copyright©2021, American Chemical Society.[81]

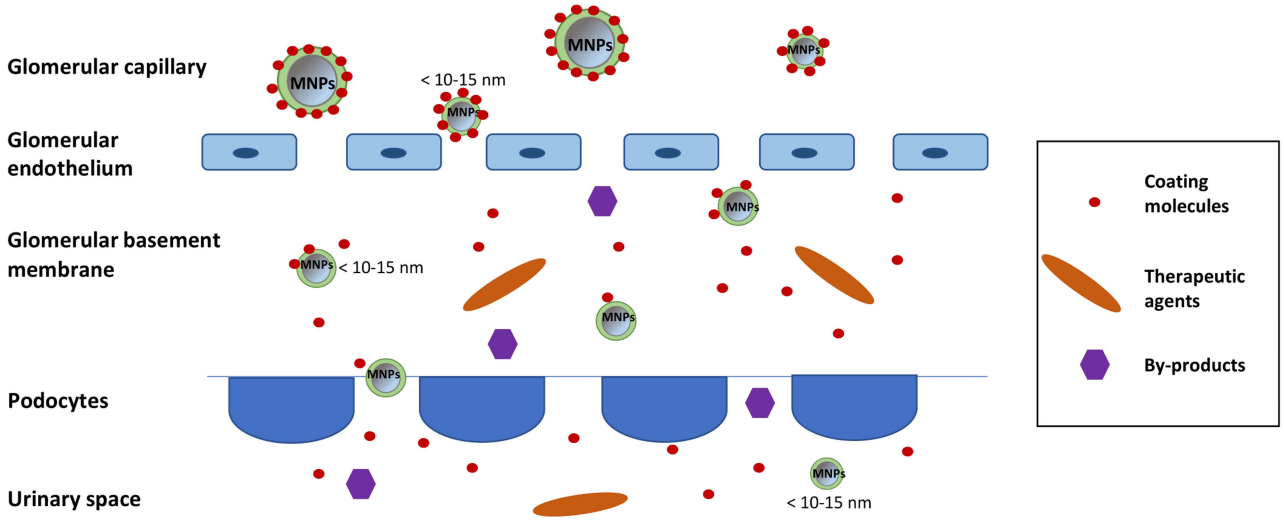

Figure 6 Extraction pathway of the MNPs or their degradation products through the kidney. MNPs smaller than 10–15 nm, the released coating molecules, degradation by-products, and therapeutic agents can cross the GMB and pores between podocytes and enter the urinary space.

main distribution sites of such nanoparticles. However, it is supposed that it could have been, for example, the result of the loss of coating molecules by magnetite 10 nm-sized cores.

Lungs

The respiratory part of the respiratory system includes bronchial tubes, alveolar ducts, and pulmonary alveoli.[85] During respiration, oxygen enters the lungs by diffusion through the capillaries surrounding each alveolar sac. Pulmonary macrophages are present in the alveoli. They can be observed in the interalveolar septa (interstitial macrophages) and inside and on the surface of the pulmonary epithelium (alveolar macrophages) surface. These cells phagocytose foreign bodies and induce an immune response. Alveolar macrophages often leave the alveoli and travel to the bronchioles, moving towards the upper respiratory tract, while others enter the lymphatic system.

Until recently, it was mistakenly believed that MNPs are poorly recognized by the body's defenses and thus ineffectively removed from the lungs due to the small accumulation of phagocytes.[86] It has been demonstrated that pulmonary phagocytosis responds very effectively to metallic nanoparticles' deposition, including magnetic nanoparticles.[87] Nanometric MNPs are removed from the lung tissue faster than micrometric particles, probably due to more active phagocytosis of nanostructures. This is of great importance because nanoparticles administered by inhalation are deposited mainly in the lungs.

A series of studies concern the biodistribution MNPs in organs, including lungs. For example, Edge et al investigated the biodistribution of 12 nm- and 15-sized superparamagnetic iron oxide nanoparticles in pigs.[88] Using pEPR technique analysis, they observed a dose-dependent accumulation for both sizes of nanoparticles in pig lungs compared to controls after 5 hours after injection. This was confirmed by histological staining with Prussian blue, showing MNPs localized in alveolar tissue. Other studies on the biodistribution of hydroxyl-ethyl starch-coated MNPs in mice using ICP-MS have shown the presence of nanoparticles in lungs after 4 hours after intravenous injection (about 0.15 mg Fe/g tissue). However, the number of deposited MNPs decreased over time, reaching a value of about 0.1 mg Fe/g tissue after 72 h.[61] After 14 days, the nanoparticles in the lungs were undetectable This confirms the thesis that MNPs in these organs are phagocytosed rapidly, thus reducing the risk of their side effects.

Research is also being conducted on using magnetic nanoparticles as drug carriers in the lungs. For example, the heavily supplied with capillaries lung tissue was exploited to deliver positive charge-coated MNPs containing the anti-cancer drug irinotecan.[89] The endothelium is lined richly with negatively charged heparin sulfate proteoglycans[90] to bind the positively charged growth factors and proteins and positively charged nanoparticles, for example, coated with positively charged lysine. Magnetic nanoparticles were also studied as potential early diagnosis lung cancer agents.[91] Moreover, Tan et al proposed using magnetic nanoparticles by inhalation as drug carriers directly to the primary target site.[92] This allows for avoiding the risks of systemic toxicity.

Heart

Tissue-resident macrophages have also been observed in the heart. Cardiac macrophages are self-proliferating and independent of blood monocyte-derived macrophages.[93] The macrophages in the heart are very heterogeneous and show phenotypic and functional adaptation depending on the surrounding environment and aging. Two main groups can be distinguished, including classical "inflammatory" macrophages with pro-inflammatory properties (M1) and alternatively "anti-inflammatory" macrophages (M2) associated with cell proliferation and tissue repair. The essential functions of M1 macrophages are phagocytosis and destruction of bacteria, elimination of neoplastic cells, and production of pro-inflammatory cytokines.[74] However, the exact role of cardiac macrophages in removing nanoparticles still requires in-depth research and clarification.

It is worth noting that magnetic nanoparticles have been used to treat cardiological diseases such as myocardial infarction. One of the methods of treating this type of disease is using mesenchymal stem cells (MSCs) to produce exosomes (extracellular vesicles – EVs).[94–96] However, most cells diffuse out from the injection area immediately after cell injection into the infarcted heart, limiting their therapeutic potential. It was found that magnetic guidance of iron oxide nanoparticles MNPs–incorporated NVs following injection could improve the retention of NVs in the infarcted heart.[97] It was also demonstrated that apart from the enhanced retention, NVs derived from MNPs-incorporated MSCs contained much larger quantities of therapeutic molecules for cardiac repair (RNAs and proteins) than normal MSCs-derived NVs. Moreover, MNPs-NVs exhibited antiapoptotic, antifibrotic, anti-inflammatory, and proangiogenic effects on cardiac fibroblasts (CFs), cardiomyocytes (CMs), endothelial cells (ECs), and macrophages, which are the primary therapeutic mechanisms of MSCs for cardiac repair in vitro.

Notwithstanding the above, studies on the biodistribution of magnetic nanoparticles in the body indicate a low level in a short time or lack of accumulation in the heart. For example, it has been reported that magnetic particle imaging (MPI) is used to track and quantify after intravenous administration of human MNPs (Ferucarbotran)-incorporated MSCs in rats.[98] The biodistribution has shown the accumulation of MNPs mainly in the liver, but no MPI signal in the heart was detected. In other studies, the authors investigated the bioavailability of carboxy dextran-coated MNPs in different organs.[99] They reported the accumulation of nanoparticles mainly in the liver, spleen, brain, and lungs and, to a small extent, also in the heart 2 hours after injection. It is worth noting that even if, shortly after administration, nanoparticles are accumulated to a small extent in the heart, their level in this organ is undetectable in the case of biodistribution measurements after a longer time, usually after 24 hours.

Brain

The blood-brain barrier (BBB) is a characteristic central nervous system (CNS) feature. The brain microvascular endothelial cells (BMVECs) line the blood vessels tightly together by tight junctions. For this reason, the penetration of various compounds is very limited. The BBB prevents the entry into the brain of various toxins and pathogens, such as

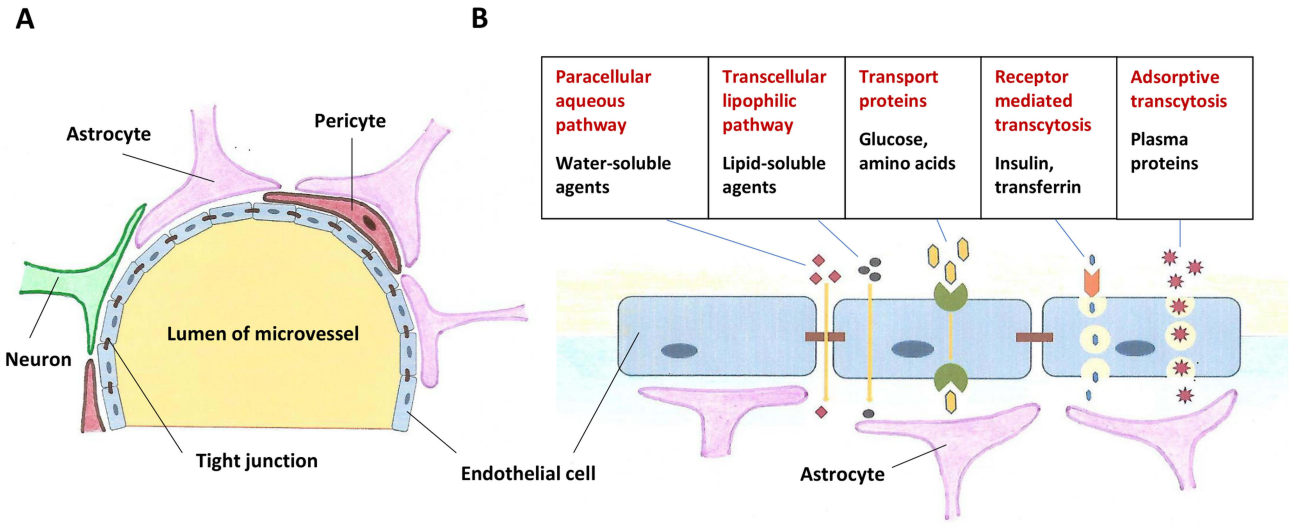

Figure 7 Structure and function of the blood-brain barrier.

bacteria, viruses, fungi and parasites, and other detrimental molecules and cells, and allows the uptake of particular nutrients and hormones only. The BBB also includes cells called pericytes and astrocytes (Figure 7A).[100,101] Pericytes are embedded into the basement membrane of microvessels and associate closely with endothelial cells. These cells are believed to provide structural support for microvessels, influence BBB permeability, and perform immune functions by detecting and destroying harmful microorganisms. They synthesize structural and signaling proteins and contribute to the BMVECs proliferation, migration, and differentiation processes.[102] The second type of cells are astrocytes that create the BBB structure contributing to the neurovascular unit. They also help recruit, among others, white blood cells to the CNS. Glial cells are immune cells that are found close to the BBB. They absorb and destroy microorganisms, another barrier against potential pathogens and toxins.

In summary, the primary function of BBB is to maintain a neutral microenvironment and protect the brain against blood-circulating microorganisms. However, BBB is semi-permeable and allows specific molecules, including, unfortunately, microbes, to penetrate through several main mechanisms.[100] The paracellular aqueous pathway allows water-soluble molecules to pass between endothelium cells (Figure 7B). In turn, lipid-soluble agents penetrate the lipophilic transcellular pathway. Molecules such as glucose, amino acids, and nucleosides use transport proteins, whereas insulin penetrates through receptor-mediated transcytosis. Albumin and other plasma proteins use adsorptive transcytosis. Microbes, in turn, use three main mechanisms:[103] pathogens can cross the barrier by direct endocytosis of endothelial cells, in the paracellular traversal model – through loosened tight junction, and by phagocytic penetration using transmigration within infected pathogens (the "Trojan horse" mechanism).

The BBB also prevents the delivery of therapeutics and nanoparticles to the brain for tumor diagnosis and treatment.[43] It turns out that if nano agents are appropriately designed, they can penetrate the BBB. Their size, charge, and coating molecules play a decisive role. For example, the functionalization of the MNPs surface with lipophilic substances improves the passive diffusion of nanoparticles into the brain parenchyma.[104] Also, attachment of ligands such as apolipoproteins,[105] transferrin antibodies and transferrin,[106,107] α-methyl tryptophan,[108] and positively charged moieties have been reported to promote receptor-mediated and adsorptive-mediated transcytosis for nanoparticles to cross the BBB. It was also reported that MNPs coated with chitosan and PEG can cross the BBB.[109] This was related to the cationic nature of chitosan interacting with the negatively charged endothelium of the brain, as well as the small size of nanoparticles and the high lipophilicity of PEG, thus enabling penetration through the endothelial cells. Another study examined the capability of using lysophosphatidic acid (LPA) to transiently disrupt the tight junctions and allow MNPs to enter the brain.[38] The studies showed improved delivery efficiency of MNPs following LPA administration to the brain (approximately 4-fold vs control); moreover, no significant activation of microglia or astrocytes was observed. On the other hand, Nadeem et al[110] reported high accumulation in the brain of the uncoated ^{99m}Tc-labelled, 10 nm-sized nanoparticles in a rabbit model. It has also been shown that dextran-coated, 30–50 nm-sized MNPs can enhance quercetin's bioavailability in the intact rat brain.[36]

Summarizing, studies on the biodistribution of magnetic nanoparticles in mammalian organisms indicate that their accumulation in the brain is sometimes observed. The rational design of MNPs and guiding them using an external magnetic field[111,112] allows for efficient diagnosis and drug delivery with these nanoparticles. However, the long-term biodistribution and clearance mechanisms of MNPs in the brain require further investigation.

Biodistribution of Magnetic Nanoparticles in Tumors

Cancer cells can take control of the angiogenesis process, ie, the formation of new vessels, to provide enough oxygen and nutrition for tumor growth. The formation of new blood vessels in a tumor enables its local progress and the formation of distant metastases.[113] The stimulation of angiogenesis is caused by the imbalance between the factors stimulating and inhibiting this process and the most critical factor influencing the formation of new blood vessels in the vascular endothelial growth factor VEGF. In a cancerous tumor, newly formed vessels are arranged unevenly, forming numerous branches. They are characterized by changing diameters. In the walls of these vessels, there is a lack of innervation, some of the receptors, or smooth muscle endothelium (pericytes).

An essential feature of new blood vessels is their increased permeability.[114] Leaky tumor blood vessels with pores in the endothelium with a diameter of up to several micrometers are the basis of the phenomenon known as enhanced

permeability and retention (EPR), which enables effective delivery of drugs or radioisotopes immobilized on MNPs to solid tumors.[115] Thus, the desired nanoparticle should preferably be in the range of 20–100 nm to avoid renal clearance[44,80] and macrophage phagocyte system (MPS)[116,117] and be able to enter the tumors by EPR.

The use of perforated blood vessels to penetrate nanoparticles described above is a part of the so-called passive targeting mechanism. However, MNPs can be decorated by tumor-specific antibodies and directed to the specific receptor molecules found in tumor cells.[118] There are also reports that MNPs functionalized with tumor-homing peptides can specifically bind to fibrin in tumor vessels and block blood flow, causing subsequent inhibition of tumor growth.[119] Also guides the MNPs to the tumor sites by external magnetic field[111,112] belongs to the so-called active targeting mechanisms.

There are many reports regarding the use of functionalized nanoparticles in the diagnostic and treatment, for example, by drug delivery to neoplastic tumors. For example, Jaiswal et al studied the efficacy of magnetic nanoparticles incorporated into poly(N-isopropylacrylamide)-chitosan nanohydrogels in inhibiting the growth of tumors in fibrosarcoma-bearing mice models.[120] The formulation was administered intratumorally to maintain the desired concentration level within the tumor mass. The study's results revealed the high efficacy of magnetic nanohydrogels in suppressing tumor growth via magnetic hyperthermia. In another study, it was reported that LTVSPWY peptide-modified PEGylated chitosan (CS)-coated magnetic nanoparticles were more actively accumulated within the area of the tumor in a short time (1 hour) as well as after 96 hours compared to PEG-CS-coated MNPs.[121] The results indicated that active tumor targeting using a tumor-specific ligand was much faster and more efficient than passive targeting based on tumor permeation, uptake, and retention. Hence, LTVSPWY-PEG-CS-modified magnetic nanoparticles could be delivered to tumors by both passive and active targeting mechanisms under in vivo conditions.

On the other hand, Tietze et al used phosphate starch-coated magnetic iron oxide nanoparticles directed to the tested tumor in rabbits using an external magnetic field (magnetic drug targeting, MDT).[62] The results showed that after intra-arterial administration of nanoparticles and MDT application, MNPs accumulated in the tumor to a greater extent than after intravenous injection. In another study, MNPs were coupled to mitoxantrone.[122] Concentrations of mitoxantrone were examined in plasma and inside the tumor 30 min after the last dose had been entirely administered. The results showed lower concentrations in the blood when a magnetic field was applied (MDT) to the tumor area, and higher doses were observed in the tumor than in the blood.

The above examples confirm that magnetic nanoparticles can be successfully accumulated in tumors using the passive targeting mechanism (increased permeability of the tumor's blood vessels) and active targeting. An active targeting mechanism by guiding MNPs using an external magnetic field increases the efficiency of nanoparticle distribution in the tumor area while reducing their concentration in the blood plasma. Also, labeling nanoparticles with peptides, antibodies, or other homing molecules significantly increases the accumulation of MNPs in specific tumors. However, it is necessary to be aware that tumors' specificity may differ depending, for example, on the site (organ) of occurrence. Therefore, the rational design of nanoparticles, the type of coating molecules, and the homing particles must be deeply studied concerning specific tumors. Moreover, nanoparticles that are expected to play a role in tumor diagnosis (Magnetic Resonance Imaging) and treatment (hypothermia, internal radiotherapy, or drug delivery) cannot be immediately captured by MPS and removed from the body. That is why it is so important to know the pharmacokinetics and biodistribution of specific nanoparticles and also, in this respect, to design nanoparticles of a specific size and coating molecules.

Factors Affecting Biodistribution of Magnetic Nanoparticles

As we recently discussed in our review, the progress in the research on the use of magnetic nanoparticles for biomedical applications has shown that their pharmacokinetics are influenced by the size, shape, charge, and, above all, surface chemistry of the nanostructures.[123] Similar factors determine biodistribution MNPs in body organs.

Size and Morphology of MNPs

Detailed studies confirm that the hydrodynamic diameter of nanoparticles (d_H) affects both their pharmacokinetics and biodistribution in different organs.[33,124,125] $D_{H,}$ usually measured using DLS (Dynamic Light Scattering), is the size of MNPs, including any solvent molecules attached to their surface.[126] Generally, the results of studies investigating the size

effect on the MNPs biodistribution are analogous to those found for other types of nanoparticles (for example polymeric NPs)[127] and suggest that larger MNPs are taken up faster by the liver and spleen and have shorter circulation time (and thereby half-life) in the blood. In contrast, smaller MNPs accumulate mainly in the lymph nodes and, to a lesser extent, in other organs having longer circulation time. This is confirmed by the study, which it was compared the biodistribution of Ferumoxtran-10 with the earlier reported biodistribution of Ferumoxides[128] – MRI agents with similar dextran-coating but different sizes: d_H = 15–50 nm and 62–80 nm, respectively.[129–131] In rats, 30 nm-sized Ferumoxtran-10 nanoparticles were mainly localized in the spleen: 37–46% of the injected dose (ID), liver (25% ID), and lymph nodes (5–11% ID) 24 hours after intravenous injection, whereas 80 nm-sized nanoparticles of Ferumoxides had predominant liver accumulation (83% ID at 1 h post-injection and >50% ID after 24 h).[132] The results of these studies are in agreement with those of others where it has been studied the biodistribution of dextran-coated MNPs with sizes in the range of 33 to 99 nm.[133] It has been reported a similar trend: the higher distribution level of larger MNPs in the liver. In another study, the biodistribution of PEG-coated MNPs with the sizes of d_H=16.5 and 35.8 nm was analyzed.[125] The results demonstrated that both types of MNPs tended to be distributed primarily in the liver and spleen, while in other organs such as the lungs, heart, and kidneys, the presence of MNPs was found in smaller amounts. The accumulation of larger nanoparticles was slightly higher in the liver and lungs than in the case of smaller MNPs, and much less in the heart and kidneys. On the other hand, MNPs with a size of 16.5 nm achieved higher tumor uptake.

Despite the general trend outlined above, it should be considered that the pharmacokinetics, biodistribution, and elimination of nanoparticles are the result of many factors such as, among others, size, but also charge, and surface chemistry. For this reason, the results of size-dependent biodistribution may differ for a specific type of nanoparticle. Citing the detailed results as an example, the worth mentioning is the evaluation of carboxyl-coated MNPs in vivo to systematically assess their size-dependent (10, 20, 30, 40 nm MPNs) biodistribution in mice.[44] The results showed that the smallest MNPs (10 nm) showed the highest uptake in the liver, whereas the largest MNPs (40 nm) showed the highest uptake in the spleen on day 1 post-injection. The 10 nm IOMNs were also more quickly cleared from the kidney and readily penetrated the BBB. The iron content was significantly lower in the heart of mice treated with MNPs than in the control mice.

The findings regarding the influence of the MNPs' size on their biodistribution concern mainly spherically shaped nanoparticles. However, not only the size but also the shape of MNPs affect their accumulation in different organs. Studies on how the shape contributes to the biological effect of nanomaterials are limited. There are few reports on shape's impact on nanomaterials' biological performance. One of them presents magnetic mesoporous silica nanoparticles (M-MSNPs) with different aspect ratios (AR=1, 2, and 4; spheres and nanorods).[134] Biodistribution studies have shown that the shape of the nanostructures played a crucial role in the ability of M-MSNPs to accumulate in various tissues. M-MSNPs nanorods accumulated most in the spleen compared to all nanostructures tested, while the spherical M-MSNPs accumulated mainly in the liver. M-MSNPs with the highest aspect ratio in neoplastic tumors were predominantly present, while spherical M-MSNPs accumulated in the tumor the least efficiently. The authors of the discussed studies hypothesized that the significant accumulation of nanorods in the tumor was due to the larger surface area of this type of nanomaterials compared to spheres, which led to a slower clearance rate. Moreover, it is most likely related to the fact that a sizeable length-to-weight ratio translates into longer nanoparticle circulation time caused by the lesser macrophage uptake.[42,135,136] Thus, non-spherical MNPs accumulate in the target tissues more efficiently.

More details on the biodistribution of MNPs of different sizes are provided in Table 1.

Surface Charge

The surface charge also determines biodistribution and interaction with other biological environments. Magnetic iron oxide nanoparticles with a neutral surface charge exhibit longer circulation time and reduced uptake via RES organs due to decreased opsonization. Positively charged nanoparticles are generally more easily internalized than neutral and negatively charged nanoparticles due to strong interactions with biological membranes.[142] For example, Papisov et al studied the effect of surface charge on the biodistribution of two types of functionalized MNPs: the positively charged (poly-lysine)-dextran-coated MNPs and negatively charged succinate-(poly-lysine)-dextran-coated MNPs.[140] The positively charged MNPs showed faster clearance. They were found mainly in the liver and spleen, whereas the negative ones

Table 1 Biodistribution of Magnetic Iron Oxide Nanoparticles (MNPs) of Different Sizes and Coated with the Different Types of Molecules in Mammal Models

Core/ Hydrodynamic Size	Coating Molecule	Animal Model	Dose	Administration Method	Technique	Main Sites of Biodistribution (Fe/g of Tissue; Fe/dl of Tissue; Fe/mm^2 of Tissue)	Toxicity	Ref.
10–11 /- nm	Curcumin	Mouse	5 mg/kg in 6 repeated doses	Intravenous injection	AAS[a]	Spleen and brain (≈ 0.11 mg Fe/dl); 3 days after final injection	No pathological changes in the integrity of the spleen, liver, kidney or brain	[34]
11/85 nm	Glc[b]-PMAO[c]	Mouse	0.15 mg Fe/tumor	Intratumor injection	AC magnetic susceptibility	Tumor, skin next to the tumor, spleen, liver (≈ 0.1–0.3 mg Fe/g); 30 days after injection	-	[137]
11/193 nm	Oleic acid-Pluronic	Rat	10 mg Fe/g	Intravenous injection	ICP-MS[d]	Spleen (≈ 1.2 mg Fe/g); 21 days after injection	Transient increase in oxidative stress which did not affect cellular integrity and tissue morphology	[35]
a) -/20 nm b) -/110 nm	Starch	Mouse	80 mg Fe/kg	Intravenous injection	ICP-MS	a) Spleen (≈ 2.5 mg Fe/g); liver (≈ 1.0 mg Fe/g); b) Spleen (≈ 2.3 mg Fe/g); liver (≈ 1.6 mg Fe/g); 3 days after injection	-	[61]
10/47 nm	Polyacrylic acid	Mouse	a) 8 mg Fe/g b) 20 mg Fe/g c) 50 mg Fe/g	Intravenous injection	AAS	a) Spleen (≈ 1 mg Fe/g); liver (≈ 1 mg Fe/g); lungs (≈ 0.4 mg Fe/g); b) Spleen (≈ 1.7 mg Fe/g); liver (≈ 1.25 mg Fe/g); lungs (≈0.38 mg Fe/g); c) Spleen (≈ 3 mg Fe/g); liver (≈ 2.3 mg Fe/g); lungs (≈ 0.055 mg Fe/g); 24 hours after injection	Increased hepatic lipid peroxidation at the highest dose tested (50 mg Fe/g); no significant effect in the kidneys regarding lipid peroxidation	[33]
-/100-250 nm	Phosphated starch	Rabbit	-	Intraarterial injection (close to the tumor) and magnetic targeting to the tumor	Magnetorelaxometry-SQUID[e] analysis	Liver (≈ 44% of the complete iron detected); tumor (≈ 23% of the complete iron detected)	-	[62]
5/41 nm	Uncoated, ^{99m}Tc-labelled	Mouse	100 µg Fe per mouse	Intravenous	Direct counting using an HPGe[f] detector	Liver (≈ 55% of ID[g]/g); spleen (≈ 20% of ID/g); 5 minutes after injection	-	[63]
-/40 nm	PEG[h], ^{111}In-labelled	Mouse	-	Intravenous	Assay for ^{n}C using the liquid scintillation counter	Liver (≈ 37% of the radioactivity/g); spleen (≈ 21.5% of the radioactivity/g); kidney (≈ 8% of the radioactivity/g); 24 hours after injection	-	[64]

12 nm/- and 15 nm/-	DMSA[i]	Pig	a) 0.5 mg/kg b) 2 mg/kg	Intravenous	MRI[j], histology, pERP[k]	Liver and spleen (majority of the injected nanoparticles, dose dependent accumulation); lungs [a) 12 nm-sized MNPs ≈ 20 mg Fe/g, 15 nm-sized MNPs ≈ 18 mg Fe/g; b) 12 nm-sized MNPs ≈ 90 mg Fe/g, 15 nm-sized MNPs ≈ 50 mg/g]; 5 hours after injection	-	[88]
12 nm/ a) 42 nm b) 49 nm	a) DMSA b) PEG	Rat	0.44 mg Fe/kg	Intravenous	MR relaxation measurements	a) Liver (≈ 0.5 mg Fe/g); spleen and lungs (≈ 0.4 mg Fe/g); b) Liver (≈ 0.42 mg Fe/g); lungs (≈ 0.4 mg Fe/g); spleen (≈ 0.25 mg Fe/g); 3 hours after injection	No changes in the morphology of the liver, lungs and spleen	[37]
10 nm/242 nm	PAMAM[l] dendrimer	Mouse	5 mg/mL per mouse	Intraperitoneal	ICP-MS	Kidney (≈ 2.6 ppm of Fe); liver (≈ 2.0 ppm of Fe); lungs and heart (≈ 1.5 ppm of Fe); tumor (≈ 1.2 ppm of Fe); 4 hours after injection	No significant blood parameters and renal function indicators' changes in the case of chronic exposure to the dose of 100 mg/kg; non-significant increase in ALP and ALT enzymes; significant increase in direct bilirubin at the dose of 10 mg/kg	[84]
-/29 nm	EDT[m]	Mouse	5 mg Fe/kg	Intravenous	ICP-OES[n]	Liver (≈ 80% of ID); spleen (≈ 10% of ID); brain (≈ 3.6% of ID); 30 minutes after injection	Minimal inflammatory effects following delivery of nanoparticles to the brain	[38]
Nanoworms; 5 nm core, 50 nm length/66 nm	dextran	Mouse	3 mg/kg Fe	Intravenous	Magnetorelaxometry-SQUID analysis	Lymph nodes (≈ 40% of ID/g); spleen (≈ 15% of ID/g); liver (≈ 10% of ID); 24 hours after injection	-	[138]
10 nm/-	APTES[o]	Mouse	a) 50 mg/kg b) 100 mg/kg	Intraperitoneal	ICP-MS, histology	a) Spleen (≈ 0.43 mg Fe/kg); liver (≈ 0.2 mg Fe/kg); b) Spleen (≈ 0.5 mg Fe/kg); liver (≈ 0.28 mg Fe/kg); 7 days after injection	Transient increase in AST and LDH enzymes level; transient increase for BUN; Serum TP levels within the normal range; no significant damage, inflammation and any pathological changes in important organs	[39]
70–80 nm/-	PEG-PAMAM dendrimer	Mouse	40 mg/kg	Intravenous	CLSM[p]	Liver and spleen (≈ 0.16 mg Fe/g); lungs (≈ 0.75 mg Fe/g); heart (≈ 0.5 mg Fe/g); 24 hours after injection	Most parameters of various cytokines and enzymes within the normal range; no significant changes in enzymes reflective of inflammatory response or organ toxicity	[40]

(*Continued*)

Table 1 (Continued).

Core/ Hydrodynamic Size	Coating Molecule	Animal Model	Dose	Administration Method	Technique	Main Sites of Biodistribution (Fe/g of Tissue; Fe/dl of Tissue; Fe/mm^2 of Tissue)	Toxicity	Ref.
-/302 nm	PEG-modified thiolated gelatin – ^{111}In-labelled	Mouse	2 μCi/200 μL per mouse	Intravenous	Radioactivity measurements	Kidneys (≈ 45% of radioactivity/g); spleen (≈ 25% radioactivity/g); liver (≈ 20% radioactivity/g); tumor (≈ 5% radioactivity/g); 24 hours after injection	-	[139]
10nm/-	Uncoated, ^{99m}Tc-labelled	Rabbit	200 μg/mL per rabbit	Intravenous	SPECT[r]	Heart, lung, kidney, brain (≈ 30% of concentration activity in the brain normalized over the whole-body activity concentration); after 2 hours after injection; more detailed data were not provided	-	[110]
30–50 nm/-	Dextran-quercetin	Rat	100 mg/kg	Oral	ICP-OES	Brain (≈ 6.2 μg/g) after 24 hours after administration; distribution to other organs has not been studied	No histological alterations in the liver tissue	[36]
4.4–6 nm/22±6 nm	Dextran, ^{111}In-labelled	Rat	2 μg/kg – 100 mg/kg	Intravenous	Radioactivity measurements	Lymph nodes: a) mesenteric, para-aortic group (≈ 30–50% of ID/g) b) popliteal, axillary groups (≈ 10–20% of ID/g) c) cervical, thoracic, other node groups (≈ 2–20% of ID/g); liver (≈ 1.5–2% of ID/g); other tissues (< 0.2% of ID/g); 24 hours after injection	-	[140]
-/80 nm	Dextran, ^{59}Fe labelling	Rat	1 mg Fe/kg	Intravenous	Radioactivity measurements	Liver (≈ 82.6% of ID or ≈ 6.3 of ID/g); spleen (≈ 6.2% of ID or ≈ 10.9% of ID/g); minimal amounts in other tissues; 1 hour after injection	-	[133]
-/110 nm	Starch	Rat	12–25 mg Fe/kg	Intravenous; magnetically targeted to brain tumors	ICP-OES and ESR[s]	ESR results: Liver (≈ 6000 nmol Fe/g); Spleen (≈ 8000 nmol Fe/g); Lung (≈ 1500 nmol Fe/g); Kidney (≈ 6.1 nmol Fe/ g); Tumor (≈ 39.2 nmol Fe/g); Normal brain (≈ 5.6 nmol Fe/g); 50 minutes after injection	-	[141]

a) 10 nm/- b) 50 nm/-	Uncoated	Rat	500 mg/kg 3 times a week for 5 weeks	Intraperitoneal	AAS and pEPR	AAS results: a) Liver (≈ 5000 mg Fe/kg); spleen (≈ 9000 Fe mg/kg); b) Liver (≈ 5000 mg Fe/kg; spleen (≈11,500 mg Fe/kg) pEPR results: a) Liver (≈ 2500 mg Fe/kg); spleen (≈ 7000 mg Fe/kg); b) Liver (≈ 3200 mg Fe/kg); spleen (≈ 8000 mg Fe/kg) after 5 weeks; distribution to other organs has not been studied	Histological pathological changes in the liver (decomplexation of hepatic tubules, cytolysis observed in some places); extensive deposits of lumps of iron-containing pigment in the red pulp of the spleen	[41]

Note: Dashes in some of the table cells indicate that the data was not available in the source articles.

Abbreviations: [a]AAS, Atomic Absorption Spectroscopy; [b]Glc, glucose; [c]PMAO, poly(maleic anhydride-alt-1-octadecene); [d]ICP-MS, Inductively Coupled Plasma, Mass Spectroscopy; [e]SQUID - Superconducting Quantum Interference Device; [f]HPGe, High Purity Germanium; [g]PEG, polyethylene glycol; [h]ID, injected dose; [i]DMSA, dimercaptosuccinic acid; [j]MRI, Magnetic Resonance Imaging; [k]pERP, particle Electron Paramagnetic Resonance; [l]PAMAM, poly(amidoamine); [m]EDT- ethylenediamine triacetate; [n]ICP-OES - Inductively Coupled Plasma Optical Emission Spectrometry; [o]APTES, (3-aminopropyl)triethoxysilane; [p]CLSM, Confocal Laser Scanning Microscope; [q]MPI- Magnetic Particle Imaging; [r]SPECT, Single-Photon Emission Computed Tomography; [s]ESR, Electron Spin Resonance.

https://doi.org/10.2147/IJN.S415063

accumulated in lymph nodes, thus showing more similar biodistribution to the nearly neutrally charged dextran-coated MNPs. Another study found that both negatively and positively charged MNPs showed increased liver uptake compared to neutrally charged MNPs.[133] On the other hand, Sun et al studied the biodistribution of MNPs coated with negatively charged ethylenediaminetetraacetate (EDT) as the most likely candidates for the BBB crossing to enhance the delivery of MNPs in the brain.[38] The selection of negatively charged MNPs-EDT was based on several previous findings. Firstly, negatively charged nanoparticles have improved colloidal stability[143] and lower levels of non-specific cell association compared to positively charged MNPs.[144] Secondly, MNPs-EDT in vitro cell culture models were significantly more permeable than positively charged MNPs following osmotic disruption and magnetic field applications.[145]

Coating Molecules and Protein Binding

Coating molecules on the MNPs surface affect their size and charge, influencing their biodistribution described in previous chapters. However, it is essential to consider the complexity of the process as surface chemistry also affects the binding protein profile, and the binding proteins influence biodistribution. A binding protein can cause additional changes in nanoparticle size and charge, affecting the internalization process of MNPs into macrophages and the overall distribution in the body.[146–148]

Specific bound proteins, such as IgG, complement factors, and fibrinogen, allow macrophages of RES to recognize nanoparticles and promote phagocytosis more easily.[149,150] The particles coated with these proteins tend to accumulate in the liver and spleen. For imaging and drug delivery to body areas other than RES organs, MNPs must have a longer circulation time in the blood and reduced flow through the RES organs. The polymers that give the MNPs an anti-fouling character and enable their increased uptake to the site of interest are different variations of polyethylene glycol (PEG) or poly(ethylene oxide) (PEO)-containing chemical groups.[151–154] Generally, PEGylation is the most common method of masking nanoparticles from immune recognition.[155] It has been shown to decrease interactions of nanoparticles with blood proteins and help avoid recognition by RES, thus prolonging circulation time in blood and making it easier to reach organs other than the liver and spleen. For example, Liu et al[156] developed single-core Fe_3O_4 MPI tracers coated with covalently bonded PEG-silane brushes. The newly tailored tracer had MPI sensitivity about three times higher than the commercial tracer Ferucarbotran and 3 minutes after injection in the mice model, the tracer was seen to be distributed throughout the body, with the most significant signal corresponding to the heart. There are also studies showing that PEG-coated can effectively distribute to the tumors. For example, MNPs with a crosslinked starch and PEG coating showed increased circulation time (up to 12 h) and distribution in the tumor.[152]

PEG and many other coating polymers and molecules and their effect on biodistribution in the body were tested. For example, a high signal from Pluronic-oleic acid-MNPs was reported at the tumor site on the second day after administration.[16] Jain et al[35] developed iron oxide MNPs coated with both oleic acid (OA) and Pluronic that can be loaded with high doses of hydrophobic drugs[157] and studied their biodistribution in rats. The maximum iron level was observed in the liver after 6 h (55% of the total injected iron), which was only 20% after one day. These MNPs have been accumulated in other organs, mainly in the spleen, lungs, kidneys, heart, and brain. Another study determined the concentration of MNPs coated with oxidized starch and their degradation products in Kupffer, endothelial and parenchymal cells of the rat liver.[158] Even though the nanoparticles had a small size and quite prolonged circulation time, approximately 80% of the injected MNPs were taken up by the liver within 24 h after single-dose administration. It is worth mentioning that nanoparticles exhibited negative zeta potential because of the coating by the oxidized starch. Therefore it can be assumed that the uptake of the tested nanoparticles was mediated by scavenger receptors expressed in Kupffer cells and liver endothelial cells, binding ligands with clusters of negative charge. Ikeda et al[159] synthesized activatable fluorescence agents of dextran-coated MNPs at various molecular ratios and hydrodynamic diameters (34.1–35.9 nm). The most significant signal intensity in biodistribution studies was observed in the liver, followed by the spleen. When an excessive amount of nanoparticles were administered, a portion of the circulating MNPs was taken up by macrophages in the liver and spleen, and the excess was detected in other tissues, such as the lungs and adipose tissue, where macrophages are substantial.[50] On the other hand, there were developed theranostic hybrid MNPs with carbon shells and a hydrodynamic diameter of about 16 nm.[160] Biodistribution studies have shown that nanostructures were mainly accumulated in the liver through the RES system. However, the carbon-shell MNPs were also detected in the

kidneys, spleen, lungs, heart, and tumors. There were also developed dextran-coated ultrasmall iron oxide nanoparticles coated with peptides containing L-arginine–glycine–aspartate (Arg- Gly-Asp, RGD)[161] and aspartic acid–glycine–arginine (Asn-Gly-Arg, NGR)[162] as potential double-targeting agents in tumor angiogenesis magnetic resonance imaging (MRI).[163] The peptides bind specifically on the endothelial cells' surface in tumor neovascularization resulting in the regulation of angiogenesis, tumor growth, and metastasis.[164–166] The number of nanostructures in tumor tissues increased 1.83 times compared with the control group. However, they also accumulated in the kidney, liver, and spleen. Salimi et al[84] synthesized MNPs coated with the fourth generation (G4) of polyamidoamine (PAMAM) dendrimer and the amino groups of dendrimer molecules were next conjugated with mPEG.[167,168] At 24 h after injection in the mice model, the maximum amount of the nanostructures was found in the lung and kidney tissues. The results showed decreased PAMAM-PEG coated nanoparticles' biodistribution in all tissues 8 h after administration. The iron level was reduced by about half from the initial dose except for the lungs, where the iron content decreased by 14%. The authors explained that this phenomenon could be the return of nanoparticles to the bloodstream and then uptake to the spleen or lymph nodes. At the same time, the lung immune system acted as the main barrier against PAMAM-PEG-coated MNPs and prevented them from returning to the bloodstream and other organs.[169] It also evaluated the biodistribution of three types of MNPs that were coated with a carboxyl group, carboxyl group followed by PEG coating, and carboxyl group followed by BSA coating, all in the range of sizes 54–62 nm.[170] The studies conducted in rats have shown that the iron content in the kidneys, intestine, and testis did not show a significant difference compared with the control group. PEG–MNPs and COOH–MNPNs accumulated in the liver and lung. BSA-coated MNPs showed more accumulation in blood than PEG–MNPs and COOH–MNPs, which indicated that naturally occurring compounds, such as BSA, were more suitable for surface modification. After 24-day recovery, BSA–MNPs had longer-term retention time in blood, and PEG–MNPs seemed to have more accumulation ability in various organs than MNPs coated with BSA. Thus, the authors demonstrated that surface modifications played an essential role in the biodistribution of magnetic nanoparticles.

More details on the biodistribution of MNPs with different coatings are provided in Table 1.

The Effect of MNPs Vectorization

Detection, drug delivery, and imaging (MRI) by MNPs are typically limited to regions rich in the mononuclear phagocyte system, such as the liver and spleen. However, using an external magnetic field allows directing of magnetic nanoparticles to specific body sites. Another approach to achieve targeted drug delivery, especially to tumors, consists of grafting functional groups on the surface of MNPs with ligands that recognize specific receptors or biomarkers. Typically, these ligands are oligosaccharides,[171] peptides and proteins[172–179] (eg, insulin, RGD peptides, transferrins), antibodies or their fragments,[180–183] mimetics,[184] as well as vitamins such as folates that interact with tumor cell receptors.[185,186] This facilitates the biodistribution of MNPs into specific body regions. Furthermore, the antibodies labeled with low doses of radionuclides and immobilized on MNPs are used in radioimmunotherapy (RI).[187] Additionally, fluorophores anchored on the surface of nanoparticles are useful in imaging and diagnosis by using various diagnostic techniques.

More specific information concerning selected targeting agents immobilized on functionalized MNPs is presented in Table 2.

Technical Aspects

Some technical aspects, such as the way of administration, can influence the biodistribution of MNPs in the body. The most common is an intravenous injection. However, several reports describe using MNPs coated with organic shells in oral administration. One of them concerns using MNPs as contrast agents for the gastrointestinal tract.[189] In another study, a novel drug delivery system was reported composed of layer-by-layer milk protein casein-coated iron oxide nanoparticles with high stability in the stomach and enzyme-response release in the small intestine.[190] It was also reported using a nanocomposite, phytic acid-chitosan-magnetic iron oxide nanoparticles in treating colon cancer.[191] However, the studies on the biodistribution of MNPs after oral administration are very limited. Generally, MNPs must pass the transport barrier of the intestinal epithelium, and the following can cross the liver sinusoids and then gain entry to the central blood circulation system. Thus the liver is the major accumulation and clearance organ in the oral administration of MNPs, whereas the nanoparticles remaining in the digestive system are extracted through the feces.[192]

Table 2 MNPs Decorated with Targeting Agents

Type of Targeting Agent	Specific Targeting Agent	Target	Coating	Application	Ref.
Proteins	Transferrin	Transferrin receptor	DMSA[a]	Brain glioma imaging	[175]
			Chitosan/Doxorubicin	Drug delivery	[176]
			Dextran-spermine	Drug delivery by BBB[b]	[177]
	Lactoferrin (family of transferrins)	Lipoprotein receptor-related protein	PMAO[c]	Drug deliver by BBB (glioma cells)	[178]
Peptides	GRGD[d]-peptide	αvβ 3 integrin	3-Aminopropylsilane	Not specified	[172]
	CRGD[d]-peptide		PEG[e]	Imaging and drug delivery	[173]
	Insulin	Human fibroblasts' receptors	Sodium oleate	Drug delivery	[179]
Antibodies	SM5-1 monoclonal antibody	Hepatocellular carcinoma cells	Dextran	Targeted contrast agent for diagnosis of hepatocellular carcinoma cells	[180]
	Anti-transferrin receptor antibody OX26	Transferrin receptor	MNPs enveloped in a PEGylated bilayer to form liposomes	Drug delivery to the brain	[181,182]
	Anti-EGF[f] monoclonal antibody	EGF-receptor	PEG	Detection of lung cancer using MRI	[183]
Other molecules	Sialyl Lewis^x (sLe^x)	E-selectin (leukocytes)	Dextran	MRI diagnosis of inflammation	[184]
	Folic acid	Folate receptor	APTES[g]/PEG	Chemotherapy and hyperthermia	[185]
			Polyethyleneimine	Tumor targeting MRI	[186]
	Hyaluronic acid	CD44 antigen	Polymeric micelles using hyaluronic acid -C_{16} copolymers	MRI and photothermal-chemotherapy	[188]

Abbreviations: [a]DMSA, dimercaptosuccinic acid; [b]BBB, Blood Brain Barrier; [c]PMAO, Poly(maleic anhydride-alt-1-octadecene); [d]RGD-peptides family, L-Arg-Gly-L-Asp; [e]PEG, Polyethylene glycol; [f]EGF, Epidermal Growth Factor; [g]APTES, (3-Aminopropyl)triethoxysilane.

In the case of subcutaneous or intratumoral administration, as a general rule, the injected nanoparticles need to be small (60 nm or less).[193] These small particles injected locally infiltrate the interstitial spaces around the injection and are absorbed by the lymphatic capillary system.[194]

Regarding the intraperitoneal administration, it was tested biodistribution in a rat model of naked Fe_3O_4 nanoparticles of three sizes: 20, 50, and 1000 nm using, among others, Atomic Absorption Microscopy (AAS).[41] The results showed a high accumulation of 10– and 50 nm-sized MNPs in the spleen, followed by the liver. In comparison, micrometric particles (1000 nm) were distributed only slightly and statistically insignificantly compared to the organs of control rats.

Nanoparticles administered by inhalation or intratracheally are introduced into the alveolar spaces and mainly used for diagnosing and treating lung diseases.[169,195] For example, studies in mice have shown that inhaled MNPs accumulate in the central region of the lung about 2.5 times more efficiently than in the peripheral zones of this organ. MNPs are phagocytized by macrophages in the alveolar spaces, and their by-products are released into the pulmonary lymphatics.[196,197]

Another technical factor with a significant influence on the biodistribution of nanoparticles is the use of an external magnetic field to guide MNPs to specific sites, eg, tumors. For example, it investigated the biodistribution of[122] Iod-labelled ferrofluids (about 100 nm MNPs coated with hydrophilic starch) in vivo in rabbits.[198] The results of studies showed that ferrofluid concentration was dependent on the strength of the magnetic field. In addition, after using the focused external magnetic field, the scintigraphically detected[122] Iodine signal after intra-arterial administration to the tumor in the left femoral artery was significantly higher than administration without the magnetic field. After 10 and 60

minutes after administration of the nanoparticles, 77% and 22% of their initial activity in the tumor area were found, respectively, in the case of the application of an external magnetic field, while only 40% and 11%, respectively, in the absence of a magnet. In another study, the histology method investigated the effects of an external magnetic field on the biodistribution of MNPs in a rat model.[199] The dextran-coated Fe_3O_4 MNPs (250 nm) functionalized with the -COOH group were administered intravenously. Biodistribution studies showed accumulation of MNPs mainly in the liver and spleen in the case of the control (without magnet). When the magnetic field was applied to the right kidney, MNPs were retained over both kidneys with more of the right side. Other organ tissues close to the right kidney (ie, stomach, small intestine, and colon) did not have significant retention of MNPs.

There was also studied on the effect of anesthesia on MNPs' biodistribution after MNPs' intravenous injection.[200] For example, animals (murine) were anesthetized with isoflurane (0.5% in oxygen) or by intraperitoneal injection with a mixture of ketamine and xylazine. Then, dimercaptosuccinic acid-coated MNPs were intravenously injected. The number of MNPs in the liver and lung tissue was measured using the Alternating Current Magnetic Susceptibility method. The results have shown that the accumulation of nanoparticles in the liver was not affected by the method of anesthesia. However, the number of particles that reached the lungs for inhaled isoflurane was three times less than for the intraperitoneally injected anesthetic. In conclusion, this parameter (the type of anesthesia) must be considered when comparing different studies on MNPs distribution.

The most important factors affecting the biodistribution of magnetic nanoparticles are summarized in Figure 8.

Biodegradation and the Fate of MNPs in the Organisms

Iron oxide magnetic nanoparticles can be removed from the body by renal clearance mechanism[201] or by MPS (phagocytic cells in the blood, tissues, lymph nodes, etc.).[125] Generally, the healthy human body contains 65% iron as hemoglobin, 4% as myoglobin, and 15–30% and 0.1% as ferritin and transferrin, respectively.[202] Ferritin is a protein that complexes Fe^{3+} iron ions and stores them in the liver, keeping the iron in an accessible and harmless form. In contrast, transferrin is a glycoprotein that regulates the concentration of iron ions in the blood plasma and transports them to the tissues.[203] The mechanism of the biodegradation of magnetic nanoparticles is believed to be analogous to the metabolism of ferritin, which is digested by lysosomal enzymes to release iron ions.[32] The excess of iron (ferrous Fe^{2+} or ferric Fe^{3+} products) is then regulated by various clearance mechanisms of the body, namely, it is integrated into either the storage or utilization pathway.[125,204]

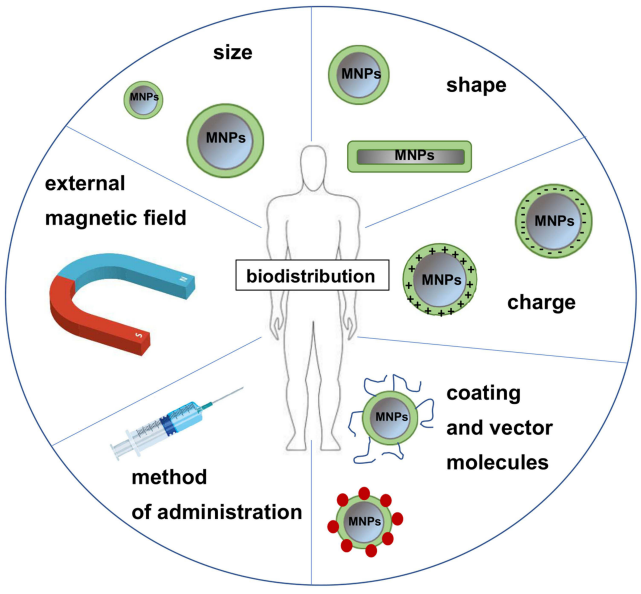

Figure 8 The main factors affecting the biodistribution of MNPs.

Intravenously administered magnetic nanoparticles are captured by macrophages, mainly of the liver and spleen, and then digested in the acidic environment of the lysosomes.[205,206] Degradation of MNPs occurs faster in the liver macrophages than in the spleen, as the former contains more iron-storing proteins.[207] The degradation rate depends on the material covering the nanoparticles[208] (hydrophilic substances favor faster degradation) as well as the dose of nanoparticles.[209] The released iron binds with apoferritin present in the cytoplasm of macrophages to form a ferritin.[79] After the iron is transported from ferritin to apotransferrin, transferrin is formed.[210] Transferrin circulates through the body supplying iron to various tissues, such as muscles, where myoglobin is biosynthesized, or bone marrow, where iron forms hemoglobin, which gets stored in the red blood cells (RBC).[79] Iron ions can be incorporated in the RBC hemoglobin as ferrous (Fe^{2+}) or ferric (Fe^{3+}) ions, albeit only ferrous ions are active in oxygen transport. Nevertheless, methemoglobin reductase can reduce iron ions in the third oxidation state to Fe^{2+} ions.[211] Therefore, there may be several alternative metabolic pathways for different forms of iron (i. a. FeO, Fe_2O_3, Fe_3O_4), which requires in-depth research.

The senescent RBCs are taken up by the red pulp of the spleen, then phagocytosed by macrophages and converted to ferritin and subsequently transferrin, which redirects iron to the bone marrow to form new erythrocytes, or to the liver, where iron is stored in hepatocytes as ferritin.[158] A certain fraction of hemoglobin is also converted to bilirubin, then excreted in urine and bile. If the body's iron content exceeds the available apoferritin, the iron forms small insoluble aggregates called hemosiderin in the liver cells, slowly releasing iron ions.[212]

MNPs can also be excreted via urine; however, nanoparticles must be small enough to utilize renal clearance, with a diameter below 10–15 nm.[201] For example, MNPs with a size in the range of 1–5.5 nm are assumed to be renal-clearable, as they can readily pass through the glomerular filtration membrane.

Nanoparticles designed for MRI or drug delivery to specific regions of the body, such as a brain tumor, must be able to cross the blood-brain barrier.[213] After fulfilling their function, the MNPs should be quickly cleared from the brain as the accumulation of nanoparticles could lead to neurotoxicity. Gu et al[214] investigated the clearance of MNPs coated with reconstituted high-density lipoprotein (HDL) and with poly(ethylene)-glycol-b-poly(lactic acid) copolymer (PEG-PLA) from the brain. They reported that the studied nanostructures were easily and rapidly cleared through the perivascular glymphatic pathway. This pathway involves astrocytes - The giant glial cells, which generally perform many functions, including participation in nerve transmission, ammonia and creatine transformations, regeneration, phagocytosis processes, and removing soluble proteins and metabolites from the brain.

Current Techniques for Analyzing the Biodistribution of Nanoparticles

The biodistribution of nanoparticles in the body means the place of their accumulation in various tissues and organs, the way they interact, their therapeutic effect, their residence time, and elimination from tissues. Knowing the biodistribution after in vivo administration of nanoparticles is essential primarily because of the target organs to which MNPs are to be delivered, but also because of undesirable accumulation and toxicity in other tissues. Therefore, the nanoparticles used in the clinic must first be thoroughly tested for biodistribution in mammalian models. Several different techniques are used for this purpose.

One of the most popular techniques for evaluating nanoparticle biodistribution is histology,[215] also known as microscopic anatomy or microanatomy. The technique involves the histological examination of tissues to determine the association of nanoparticles with the cellular microenvironment under a microscope, usually light and fluorescent. Selected tissue fragments are harvested at set time points and traditionally stained with Prussian blue dye. For example, Pham et al[216] studied the biodistribution of ultrasmall MNPs injected intraperitoneally into mice by measuring iron-positive areas in tissue sections of organs stained with this dye. In terms of advantages, histology is an inexpensive technique to study the biodistribution of nanoparticles over large sections of tissue. However, light and fluorescence microscopy generally have low resolution and cannot distinguish between individual nanoparticles in a tissue. Moreover, the technique is sensitive to human error in sample preparation and analysis techniques. Regarding fluorescence imaging, labeling MNPs with fluorescent dyes may influence their physicochemical properties and, thereby, their in vivo behavior.[217]

Another standard laboratory method is Liquid Scintillation Counting (LSC).[215] The technique quantifies the radioactivity of low-energy radioisotopes, mostly β-emitting and α-emitting isotopes.[218] LSC sample requires a mixture of the aromatic organic solvent that absorbs radioisotopic energy and scintillators ("fluors") to produce detectable light pulses. The energy released from radioactive particles excites the aromatic solvent molecules, producing excited states of electrons by scintillator molecules. Their decay to the ground state causes producing a light pulse that is characteristic of the scintillator. The emitted light is detected by the liquid scintillation counter's photomultiplier tube (PMT). For in vivo biodistribution studies, nanoparticles are labeled with isotopic markers. Organs are then harvested and prepared for LSC. The technique is sensitive, specific, and quantitative. However, an essential issue in this method is the separation of the excess of the free isotopes that did not incorporate into the nanoparticles. Moreover, LSC determines only biodistribution at the tissue or organ level but does provide any information on the specific cellular interactions.

Electron microscopy analysis provides detailed information on the biodistribution of nanoparticles under very high magnification.[219] There are different types of electron microscopy techniques, such as Transmission Electron Microscopy (TEM), Scanning Electron Microscopy (SEM), and variation of these two techniques, for example, Scanning Transmission Electron Microscopy (STEM).[215] In these techniques, the electron beam is focused by electromagnetic lenses and directed at the sample. In the case of TEM, the beam passes through the sample, while in the SEM technique, the electron beam scans the sample's surface, and the signal intensity is mapped synchronously with the scan, which allows for an enlarged image.[220] Electron microscopy provides detailed information on the biodistribution of nanoparticles, but this information is limited to a certain number of ultra-thin tissue sections. On their basis, the approximate biodistribution of MNPs in the whole organ is estimated.[215] It is worth emphasizing, however, that these techniques enable the visualization of the accumulation of nanoparticles in individual cells and organelles. The disadvantage of these techniques is their cost and time consumption. Moreover, they are used more often to determine the cellular association of nanoparticles in vitro. In contrast, the studies using electron microscopy to evaluate nanoparticle biodistribution after in vivo administration are limited.[219,221–223]

The Laser Scanning Confocal Microscope (LSCM) is used in biomedical research. Confocal microscopy is a variant of light microscopy that allows obtaining images of high magnification and resolution. The LSCM uses a laser as the light source, sensitive tube detector photomultipliers (PMTs), and a computer to control the scanning mirrors and to collect and display the images.[224] The diffraction-limited point in the sample is focused by the objective lens and scanned across by the scanning device, and thereon the point of light is detected by the PMT. The output from the PMT is embedded into the image by the computer. The LSCM method was used, among others, to determine the biodistribution of PAMAM dendrimer conjugated MNPs in mice[40] and folic acid conjugated MNPs for drug delivery (mice).[225]

Magnetic Resonance Imaging (MRI) uses strong magnets to generate a magnetic field. Under its influence, the protons in the body align with the field. MRI measures the spin magnetization of polarized protons and their respective longitudinal (T_1) and transverse (T_2) relaxation rates, resulting in high-resolution images. Contrast agents increase the speed at which protons realign and shorten the relaxation rates. Paramagnetic contrast agents reduce the longitudinal (T_1) relaxation time, which results in brighter images, whereas superparamagnetic contrast agents (MNPs) shorten the transverse relaxation rate (T_2), resulting in darker images.[226,227] On the other hand, it has been reported that MNPs smaller than 5 nm have decreased magnetic moments, which causes a strong T_2 suppression effect. Consequently, ultrasmall MNPs can be exploited as T_1 agents.[228] Generally, MRI is a direct and non-invasive technique that can determine nanoparticle biodistribution at the tissue and organ level and has unlimited penetration.[215] However, it is a relatively costly technique. Additionally, this technique can need better sensitivity.

Also, Magnetic Particle Imaging (MPI) is a diagnostic in vivo imaging method designed to image the amount and location of superparamagnetic nanoparticles in biological tissue. It makes use of the nonlinear magnetic response of the MNPs.[229] The MPI technique allows direct detection of nanoparticles, which results in greater sensitivity than magnetic resonance imaging (MRI).[230] Moreover, the intensity of the image obtained by MPI is directly related to the concentration of detected MNPs, so the technique enables the quantitative study of nanoparticles. In addition, MPI is not as expensive as MRI because it does not require an expensive superconducting magnet.[230] MPI exploits the combination of an alternating magnetic field gradient and a static magnetic field gradient for real-time. During MPI scanning, the nanoparticles are magnetized by a radio frequency (RF) magnetic field, and their time-varying magnetization induces

a time-dependent voltage across the inductively coupled receiver coil.[231,232] To sum up, MPI offers quantitative, high-contrast, and high-resolution images.

Another technique used for determining the biodistribution of MNPs is Single Photon Emission Computed Tomography (SPECT).[233] It is a non-invasive technique that produces three-dimensional images of the body by detecting gamma rays emitted from radioactive substances (which the nanoparticles must be coated with) that become localized and are taken up by specific tissues.[234,235] As the isotope decays, it emits gamma rays picked up by detectors (direct measurement). The most common radioisotopes used for SPECT imaging include ^{99m}Tc, ^{111}In, and radioiodine.[110,234,236] The biodistribution of nanoparticles can be assessed in real-time, and tissue penetration limits do not restrict the technique.[215] Conversely, it is a relatively costly technique requiring ionizing radiation exposure.

Magnetic Relaxometry (Magnetorelaxometry, MRX) can detect and locate targeted magnetic nanoparticles noninvasively without ionizing radiation. In the first phase of the magnetorelaxometric measurement, an external magnetic field of a defined strength and duration partially aligns the MNPs' moments in the direction of the field. In the second phase, just after the external field is switched off, the fading magnetic field from the decay of the sample is detected by sensitive sensors such as a superconducting quantum interference device (SQUID).[237] By this method, very sensitive detection of MNP amounts down to a few nanograms is feasible in vitro or ex vivo.[237,238] For MRX to be used in biological and medical applications, the particles must possess definitive size ranges (on the order of tens of nanometers) and have high magnetic moments.[239] This method separates nanoparticles bound to objects (for example, cells) from those that rotate in a freeway in a suspension liquid.[240] The technique's sensitivity depends on the net magnetic moments induced in the single-domain MNPs by the magnetizing pulse, the number of MNPs bound in the sample, and the sensitivity of the magnetic field sensors (such as SQUID).[239]

Electron Paramagnetic Resonance (EPR) spectroscopy, called also Electron Spin Resonance (ESR) spectroscopy can be compared to NMR (nuclear magnetic resonance) spectroscopy as both techniques use the interaction of magnetic dipoles with an applied magnetic field and electromagnetic radiation of the appropriate wavelength.[241] However, NMR relies on splitting nuclear spin states in a magnetic field, whereas EPR/ESR on splitting electronic spin states. Electron magnetic dipole arises from one or more unpaired electrons. Therefore, not all molecules are "EPR/ESR active", as the most stable molecules have a closed electronic shell. Thus, EPR/ESR spectroscopy is used to study chemical species with unpaired electrons, including paramagnetic (such as Fe(III) – transferrin), ferrimagnetic and ferromagnetic (eg, magnetite), and antiferromagnetic (eg, ferritin) materials.[242,243] Both endogenous iron-protein complexes (such as hemoglobin, transferrin, ferritin, and hemosiderin) and the exogenous MNPs can be detected and distinguished with EPR/ESR. Although the technique is appropriate to study iron oxide nanoparticles and free radicals in the biological samples,[244,245] it has not been widely utilized for biodistribution studies.[242,243] This limited use could be attributed to the technical challenge of loading tissues into a long (190 mm), narrow (3 mm) EPR/ESR tube for sample analysis.[141]

Another technique often used for determining the biodistribution and concentration of iron contained in MNPs is Atomic Absorption Spectroscopy (AAS).[33,34,41,216] AAS is an analytical technique used to determine how many specific elements are in a sample. It uses the principle that atoms and ions can absorb light of a specific wavelength. The atom absorbs this particular wavelength of light. The electrons in the atom go from the ground state to the excited state, and the amount of absorbed light is measured. In this way, the concentration of an element in the sample can be calculated.[246,247] AAS is a well-known technique. It is easy to use and provides high accuracy and sensitivity.[248,249] Importantly, AA spectrometry does not cost much to operate. The AA spectrometer can measure samples from low ppm to percentage levels over a wide concentration range. However, it can be challenging to determine elements present in very high concentrations.[248,249] Moreover, AAS does not allow for the differentiation of endogenous and administered iron.

The Alternating Current Susceptibility (ACS) is also used in the biodistribution determination of MNPs.[137] In this technique, the sample is subjected to an oscillating external magnetic field, and during this process, the magnetic moment of the sample is measured.[250] A typical measurement system consists of a permanent magnet providing a static field and a modulating coil that generates an alternating current magnetic field and produces a time-dependent magnetic moment in the sample. Only the signal induced by the magnetized sample is measured, and the background is subtracted. The ACS technique distinguishes the applied nanoparticles in the imaged tissue fragment from endogenous iron.[251] Additionally, maximum contrast for specific types of nanoparticles can be obtained by selecting specific frequencies. Moreover, ACS

provides information on the surface chemistry of MNPs and their agglomeration.[252] It has also been shown that the ACS technique can monitor the degradation of MNPs in biological media.[253]

Inductively Coupled Plasma (ICP) techniques coupled with Atomic Emission Spectroscopy (ICP-AES)[254,255] or Mass Spectroscopy (ICP-MS)[256,257] also are applied for determining of MNPs distribution. These techniques use electromagnetic induction at high temperatures, generating argon plasma, thus breaking molecular and ionic bonds in the sample. With ICP-MS, the sample is ionized, and the mass spectrometer records the mass-to-charge ratio. In the case of ICP-AS, the sample atoms are excited by plasma, and electromagnetic radiation is quantified by a spectrometer. Even though these techniques have been reported to detect iron at low concentrations, the main disadvantages of these methods are their destructive nature and the fact that they do not differentiate between endogenous and administered iron.[141]

Conclusions

The review describes the biodistribution in the body of magnetic iron oxide nanoparticles used in medicine. Thanks to their biocompatible structures MNPs are increasingly translated from laboratory research to medical applications such as drug delivery, internal radiotherapy, MRI, or hyperthermia.

In addition to their primary supermagnetic properties, MNPs also have a large specific surface area, which allows the immobilization of therapeutic agents such as drugs or radioisotopes. By utilizing functionalized and specifically decorated magnetic nanoparticles, it becomes feasible to achieve dual targeting. These nanoparticles can be directed toward specific target places in the body supported by an external magnetic field as a guiding mechanism. Furthermore, the focused application of a magnetic field allows for the limitation of MNP toxicity, thereby reducing the total amount of nanoparticles within the body.

The biodistribution of nanoparticles in the body is a parameter that determines the place and degree of the administered nanoparticle accumulation in the body. The main factors influencing the biodistribution of MNPs are their size, shape, surface charge, covering molecules and specific vectors, interaction with proteins, the route of administration, and the use of an external magnetic field. In general, biodistribution is the product of all these factors. Uncontrolled proteins attachment to MNPs (opsonization) can lead to various adverse effects, including rapid clearance from the bloodstream, hindered targeting capability, reduced bioavailability, and potential toxicity induction.

Due to the mononuclear phagocyte system, detection, drug delivery, and imaging of MNPs are typically limited to the liver, spleen, and lymph nodes. To maximize the enhanced permeability and retention (EPR) effect, it is crucial to consider the overall sizes of injected surface-functionalized iron oxide nanoparticles. Multiple studies have confirmed that nanoparticles with a size of approximately 50 nm exhibit optimal cellular uptake and slower opsonization. Larger nanoparticles exceeding 100 nm are eliminated by the reticuloendothelial system (liver and spleen), whereas nanoparticles smaller than 10 nm are cleared from the bloodstream through renal clearance.

However, applying an external magnetic field enables the targeted delivery of MNPs to specific body sites. There are many reports that the proper design of nanoparticles allows these structures to accumulate in other organs, such as the kidneys, lungs, heart, and brain. A particular challenge is to design MNPs (surface chemistry, size) to cross the BBB barrier in the brain.

Moreover, attaching ligands recognizing specific receptors or biomarkers to the functional groups on the biocompatible and biodegradable surface of MNPs facilitates the biodistribution of MNPs in specific body regions, particularly to tumor areas. The MNPs are surface coated with dextran or its derivatives for clinical application. Hydrophilic polymers, such as FDA-approved polyethylene glycol, polyphosphoesthers, and zwitterionic polymers, could also be considered.

The ligands that recognize receptors on the cells include oligosaccharides, peptides, proteins (such as insulin, RGD peptides, and transferrins), antibodies or antibody fragments, mimetics, and vitamins like folates that interact with tumor cell receptors. It has been shown that the degree of accumulation in tumors is significantly increased by applying an external magnetic field additionally.

Knowing biodistribution lets us determine if the designed nanosystems target the desired tissues and organs for therapeutic purposes. On the other hand, biodistribution studies indicate undesirable accumulation that can lead to the potential toxicity of MNPs. Therefore, studies on the biodistribution of MNPs are particularly important for clinical

applications. Addressing these limitations is crucial to further enhance the efficacy and safety of MNPs as drug delivery carriers.

Author Contributions

All authors made a significant contribution to the work reported, whether that is in the conception, study design, execution, acquisition of data, analysis, and interpretation, or all these areas; took part in drafting, revising, or critically reviewing the article; gave final approval of the version to be published; have agreed on the journal to which the article has been submitted; and agree to be accountable for all aspects of the work.

Funding

This research received no specific grant from funding agencies in the public, commercial, or not-for-profit sectors.

Disclosure

The authors declare that they have no competing financial interests or personal relationships that could have appeared to influence the work reported in this paper.

References

1. Bao Y, Sherwood JA, Sun Z. Magnetic iron oxide nanoparticles as T_1 contrast agents for magnetic resonance imaging. *J Mater Chem C*. 2018;6(6):1280–1290. doi:10.1039/C7TC05854C
2. Huang J, Zhong X, Wang L, Yang L, Mao H. Improving the magnetic resonance imaging contrast and detection methods with engineered magnetic nanoparticles. *Theranostics*. 2012;2(1):86–102. doi:10.7150/thno.4006
3. Zhou Q, Wei Y. For better or worse, iron overload by superparamagnetic iron oxide nanoparticles as a MRI contrast agent for chronic liver diseases. *Chem Res Toxicol*. 2017;30(1):73–80. doi:10.1021/acs.chemrestox.6b00298
4. Russell E, Dunne V, Russell B, et al. Impact of superparamagnetic iron oxide nanoparticles on in vitro and in vivo radiosensitisation of cancer cells. *Radiat Oncol*. 2021;16(1):104. doi:10.1186/s13014-021-01829-y
5. Palzer J, Eckstein L, Slabu I, Reisen O, Neumann UP, Roeth AA. Iron oxide nanoparticle-based hyperthermia as a treatment option in various gastrointestinal malignancies. *Nanomaterials*. 2021;11(11):3013. doi:10.3390/nano11113013
6. Obaidat IM, Narayanaswamy V, Alaabed S, Sambasivam S, Muralee Gopi CVV. Principles of magnetic hyperthermia: a focus on using multifunctional hybrid magnetic nanoparticles. *Magnetochemistry*. 2019;5(4):67. doi:10.3390/magnetochemistry5040067
7. Mu X, Li J, Yan S, et al. siRNA Delivery with stem cell membrane-coated magnetic nanoparticles for imaging-guided photothermal therapy and gene therapy. *ACS Biomater Sci Eng*. 2018;4(11):3895–3905. doi:10.1021/acsbiomaterials.8b00858
8. Eivazzadeh-Keihan R, Bahreinizad H, Amiri Z, et al. Functionalized magnetic nanoparticles for the separation and purification of proteins and peptides. *TrAC Trends Anal Chem*. 2021;141:116291. doi:10.1016/j.trac.2021.116291
9. Uskoković V, Tang S, Wu VM. Targeted magnetic separation of biomolecules and cells using earthicle-based ferrofluids. *Nanoscale*. 2019;11(23):11236–11253. doi:10.1039/C9NR01579E
10. El-Boubbou K. Magnetic iron oxide nanoparticles as drug carriers: clinical relevance. *Nanomed*. 2018;13(8):953–971. doi:10.2217/nnm-2017-0336
11. Estelrich J, Escribano E, Queralt J, Busquets M. Iron oxide nanoparticles for magnetically-guided and magnetically-responsive drug delivery. *Int J Mol Sci*. 2015;16(12):8070–8101. doi:10.3390/ijms16048070
12. Nowak-Jary J, Defort A, Kozioł JJ. Modified Physicochemical Properties of Acidic Model Drugs Immobilized on Fe3O4Magnetic Iron Oxide Nanoparticles. *Pharm Chem J*. 2020;53(11):1025–1035. doi:10.1007/s11094-020-02118-w
13. Kohler N, Sun C, Fichtenholtz A, Gunn J, Fang C, Zhang M. Methotrexate-Immobilized Poly(ethylene glycol) Magnetic Nanoparticles for MR Imaging and Drug Delivery. *Small*. 2006;2(6):785–792. doi:10.1002/smll.200600009
14. Nowak-Jary J, Machnicka B, Kozioł JJ. Cytotoxicity of chlorambucil immobilized on magnetic iron oxide nanoparticles Fe_3O_4. *Micro Nano Lett*. 2021;16(10):515–523. doi:10.1049/mna2.12080
15. Stanicki D, Vangijzegem T, Ternad I, Laurent S. An update on the applications and characteristics of magnetic iron oxide nanoparticles for drug delivery. *Expert Opin Drug Deliv*. 2022;19(3):321–335. doi:10.1080/17425247.2022.2047020
16. Foy SP, Manthe RL, Foy ST, Dimitrijevic S, Krishnamurthy N, Labhasetwar V. Optical imaging and magnetic field targeting of magnetic nanoparticles in tumors. *ACS Nano*. 2010;4(9):5217–5224. doi:10.1021/nn101427t
17. Huang X, Jain PK, El-Sayed IH, El-Sayed MA. Gold nanoparticles: interesting optical properties and recent applications in cancer diagnostics and therapy. *Nanomed*. 2007;2(5):681–693. doi:10.2217/17435889.2.5.681
18. Cheheltani R, Ezzibdeh RM, Chhour P, et al. Tunable, biodegradable gold nanoparticles as contrast agents for computed tomography and photoacoustic imaging. *Biomaterials*. 2016;102:87–97. doi:10.1016/j.biomaterials.2016.06.015
19. Retif P, Pinel S, Toussaint M, et al. Nanoparticles for Radiation Therapy Enhancement: the Key Parameters. *Theranostics*. 2015;5(9):1030–1044. doi:10.7150/thno.11642
20. Filippi L, Frantellizzi V, Chiaravalloti A, et al. Prognostic and theranostic applications of positron emission tomography for a personalized approach to metastatic castration-resistant prostate cancer. *Int J Mol Sci*. 2021;22(6):3036. doi:10.3390/ijms22063036
21. Daems N, Michiels C, Lucas S, Baatout S, Aerts A. Gold nanoparticles meet medical radionuclides. *Nucl Med Biol*. 2021;100-101:61–90. doi:10.1016/j.nucmedbio.2021.06.001

22. Pellico J, Gawne PJ, De Rosales TM. Radiolabelling of nanomaterials for medical imaging and therapy. *Chem Soc Rev*. 2021;50(5):3355–3423. doi:10.1039/D0CS00384K
23. Pérez-Medina C, Teunissen AJP, Kluza E, Mulder WJM, Van Der Meel R. Nuclear imaging approaches facilitating nanomedicine translation. *Adv Drug Deliv Rev*. 2020;154-155:123–141. doi:10.1016/j.addr.2020.07.017
24. Majkowska-Pilip A, Gawęda W, Żelechowska-Matysiak K, Wawrowicz K, Bilewicz A. Nanoparticles in Targeted Alpha Therapy. *Nanomaterials*. 2020;10(7):1366. doi:10.3390/nano10071366
25. Datta P, Ray S. Nanoparticulate formulations of radiopharmaceuticals: strategy to improve targeting and biodistribution properties. *J Label Compd Radiopharm*. 2020;63(7):333–355. doi:10.1002/jlcr.3839
26. Zhao J, Liu P, Ma J, et al. Enhancement of radiosensitization by silver nanoparticles functionalized with polyethylene glycol and aptamer As1411 for glioma irradiation therapy. *Int J Nanomedicine*. 2019;14:9483–9496. doi:10.2147/IJN.S224160
27. Chen YS, Hung YC, Liau I, Huang GS. Assessment of the in vivo toxicity of gold nanoparticles. *Nanoscale Res Lett*. 2009;4(8):858. doi:10.1007/s11671-009-9334-6
28. Cho WS, Cho M, Jeong J, et al. Acute toxicity and pharmacokinetics of 13 nm-sized PEG-coated gold nanoparticles. *Toxicol Appl Pharmacol*. 2009;236(1):16–24. doi:10.1016/j.taap.2008.12.023
29. Begines B, Ortiz T, Pérez-Aranda M, et al. Polymeric nanoparticles for drug delivery: recent developments and future prospects. *Nanomaterials*. 2020;10(7):1403. doi:10.3390/nano10071403
30. Bose A, Roy Burman D, Sikdar B, Patra P. Nanomicelles: types, properties and applications in drug delivery. *IET Nanobiotechnol*. 2021;15 (1):19–27. doi:10.1049/nbt2.12018
31. Kahraman E, Güngör S, Özsoy Y. Potential enhancement and targeting strategies of polymeric and lipid-based nanocarriers in dermal drug delivery. *Ther Deliv*. 2017;8(11):967–985. doi:10.4155/tde-2017-0075
32. Skotland T, Iversen TG, Sandvig K. New metal-based nanoparticles for intravenous use: requirements for clinical success with focus on medical imaging. *Nanomedicine Nanotechnol Biol Med*. 2010;6(6):730–737. doi:10.1016/j.nano.2010.05.002
33. Couto D, Freitas M, Costa VM, et al. Biodistribution of polyacrylic acid-coated iron oxide nanoparticles is associated with proinflammatory activation and liver toxicity: toxicity of iron oxide nanoparticles: an in vivo study. *J Appl Toxicol*. 2016;36(10):1321–1331. doi:10.1002/jat.3323
34. Aboushoushah S, Alshammari W, Darwesh R, Elbaily N. Toxicity and biodistribution assessment of curcumin-coated iron oxide nanoparticles: multidose administration. *Life Sci*. 2021;277:119625. doi:10.1016/j.lfs.2021.119625
35. Jain TK, Reddy MK, Morales MA, Leslie-Pelecky DL, Biodistribution LV. Clearance, and biocompatibility of iron oxide magnetic nanoparticles in rats. *Mol Pharm*. 2008;5(2):316–327. doi:10.1021/mp7001285
36. Enteshari Najafabadi R, Kazemipour N, Esmaeili A, Beheshti S, Nazifi S. Using superparamagnetic iron oxide nanoparticles to enhance bioavailability of quercetin in the intact rat brain. *BMC Pharmacol Toxicol*. 2018;19(1):59. doi:10.1186/s40360-018-0249-7
37. Ruiz A, Hernández Y, Cabal C, et al. Biodistribution and pharmacokinetics of uniform magnetite nanoparticles chemically modified with polyethylene glycol. *Nanoscale*. 2013;5(23):11400. doi:10.1039/c3nr01412f
38. Sun Z, Worden M, Thliveris JA, et al. Biodistribution of negatively charged iron oxide nanoparticles (IONPs) in mice and enhanced brain delivery using lysophosphatidic acid (LPA). *Nanomedicine Nanotechnol Biol Med*. 2016;12(7):1775–1784. doi:10.1016/j.nano.2016.04.008
39. Wang X, Zhang J, Yang X, et al. In vivo assessment of hepatotoxicity, nephrotoxicity and biodistribution using 3-aminopropyltriethoxysilane-coated magnetic nanoparticles (APTS-MNPs) in ICR mice. *Chin Sci Bull*. 2014;59(16):1800–1808. doi:10.1007/s11434-014-0296-4
40. Zhao H, Gu W, Ye L, Yang H. Biodistribution of PAMAM dendrimer conjugated magnetic nanoparticles in mice. *J Mater Sci Mater Med*. 2014;25(3):769–776. doi:10.1007/s10856-013-5104-1
41. Katsnelson BA, Degtyareva TD, Minigalieva II, et al. Subchronic systemic toxicity and bioaccumulation of Fe_3O_4 nano- and microparticles following repeated intraperitoneal administration to rats. *Int J Toxicol*. 2011;30(1):59–68. doi:10.1177/1091581810385149
42. Veiseh O, Gunn JW, Zhang M. Design and fabrication of magnetic nanoparticles for targeted drug delivery and imaging. *Adv Drug Deliv Rev*. 2010;62(3):284–304. doi:10.1016/j.addr.2009.11.002
43. Arami H, Khandhar A, Liggitt D, Krishnan KM. In vivo delivery, pharmacokinetics, biodistribution and toxicity of iron oxide nanoparticles. *Chem Soc Rev*. 2015;44(23):8576–8607. doi:10.1039/C5CS00541H
44. Yang L, Kuang H, Zhang W, et al. Size dependent biodistribution and toxicokinetics of iron oxide magnetic nanoparticles in mice. *Nanoscale*. 2015;7(2):625–636. doi:10.1039/C4NR05061D
45. Kawai Y, Smedsrød B, Elvevold K, Wake K. Uptake of lithium carmine by sinusoidal endothelial and Kupffer cells of the rat liver: new insights into the classical vital staining and the reticulo-endothelial system. *Cell Tissue Res*. 1998;292(2):395–410. doi:10.1007/s004410051069
46. Singh I, Vasudeva N, Mishra S. *Inderbir Singh's Textbook of Human Histology: With Colour Atlas and Practical Guide*. Jaypee, The Health Sciences Publishers; 2014.
47. Murray PJ, Wynn TA. Protective and pathogenic functions of macrophage subsets. *Nat Rev Immunol*. 2011;11(11):723–737. doi:10.1038/nri3073
48. Shi C, Pamer EG. Monocyte recruitment during infection and inflammation. *Nat Rev Immunol*. 2011;11(11):762–774. doi:10.1038/nri3070
49. Lee MJE, Veiseh O, Bhattarai N, et al. Rapid pharmacokinetic and biodistribution studies using cholorotoxin-conjugated iron oxide nanoparticles: a novel non-radioactive method. *PLoS One*. 2010;5(3):e9536. doi:10.1371/journal.pone.0009536
50. Levy M, Luciani N, Alloyeau D, et al. Long term in vivo biotransformation of iron oxide nanoparticles. *Biomaterials*. 2011;32(16):3988–3999. doi:10.1016/j.biomaterials.2011.02.031
51. Beckmann N, Cannet C, Babin AL, et al. In vivo visualization of macrophage infiltration and activity in inflammation using magnetic resonance imaging. *WIREs Nanomed Nanobiotechnology*. 2009;1(3):272–298. doi:10.1002/wnan.16
52. Weissleder R, Bogdanov A, Neuwelt EA, Papisov M. Long-circulating iron oxides for MR imaging. *Adv Drug Deliv Rev*. 1995;16(2–3):321–334. doi:10.1016/0169-409X(95)00033-4
53. Vonarbourg A, Passirani C, Saulnier P, Benoit JP. Parameters influencing the stealthiness of colloidal drug delivery systems. *Biomaterials*. 2006;27(24):4356–4373. doi:10.1016/j.biomaterials.2006.03.039
54. Owensiii D, Peppas N. Opsonization, biodistribution, and pharmacokinetics of polymeric nanoparticles. *Int J Pharm*. 2006;307(1):93–102. doi:10.1016/j.ijpharm.2005.10.010

55. Dixon LJ, Barnes M, Tang H, Pritchard MT, Nagy LE. Kupffer Cells in the Liver. In: Terjung R, editor. *Comprehensive Physiology*. 1st ed. Wiley; 2013:785–797. doi:10.1002/cphy.c120026
56. Ross MH, Pawlina W. *Histology: A Text and Atlas: With Correlated Cell and Molecular Biology*. Wolters Kluwer Health; 2020.
57. Gu L, Fang RH, Sailor MJ, Park JH. In vivo clearance and toxicity of monodisperse iron oxide nanocrystals. *ACS Nano*. 2012;6(6):4947–4954. doi:10.1021/nn300456z
58. Seested T, Appa RS, Christensen EI, et al. In vivo clearance and metabolism of recombinant activated factor VII (rFVIIa) and its complexes with plasma protease inhibitors in the liver. *Thromb Res*. 2011;127(4):356–362. doi:10.1016/j.thromres.2010.12.016
59. Lee CM, Jeong HJ, Kim SL, et al. SPION-loaded chitosan–linoleic acid nanoparticles to target hepatocytes. *Int J Pharm*. 2009;371(1–2):163–169. doi:10.1016/j.ijpharm.2008.12.021
60. Kim HR, Andrieux K, Delomenie C, et al. Analysis of plasma protein adsorption onto PEGylated nanoparticles by complementary methods: 2-DE, CE and Protein Lab-on-chip® system. *ELECTROPHORESIS*. 2007;28(13):2252–2261. doi:10.1002/elps.200600694
61. Tate JA, Petryk AA, Giustini AJ, Hoopes PJ. In Vivo Biodistribution of Iron Oxide Nanoparticles: An Overview. *Energy Based Treat Tissue Assess*. 2011;790117:384. doi:10.1117/12.876414
62. Tietze R, Jurgons R, Lyer S, et al. Quantification of drug-loaded magnetic nanoparticles in rabbit liver and tumor after in vivo administration. *J Magn Magn Mater*. 2009;321(10):1465–1468. doi:10.1016/j.jmmm.2009.02.068
63. Shanehsazzadeh S, Oghabian MA, Daha FJ, Amanlou M, Allen BJ. Biodistribution of ultra small superparamagnetic iron oxide nanoparticles in BALB mice. *J Radioanal Nucl Chem*. 2013;295(2):1517–1523. doi:10.1007/s10967-012-2173-4
64. Wang H, Kumar R, Nagesha D, Duclos RI, Sridhar S, Gatley SJ. Integrity of 111In-radiolabeled superparamagnetic iron oxide nanoparticles in the mouse. *Nucl Med Biol*. 2015;42(1):65–70. doi:10.1016/j.nucmedbio.2014.08.014
65. Yazdani F, Fattahi B, Azizi N. Synthesis of functionalized magnetite nanoparticles to use as liver targeting MRI contrast agent. *J Magn Magn Mater*. 2016;406:207–211. doi:10.1016/j.jmmm.2016.01.026
66. Zhao Z, Zhou Z, Bao J, et al. Octapod iron oxide nanoparticles as high-performance T2 contrast agents for magnetic resonance imaging. *Nat Commun*. 2013;4(1):2266. doi:10.1038/ncomms3266
67. Maeng JH, Lee DH, Jung KH, et al. Multifunctional doxorubicin loaded superparamagnetic iron oxide nanoparticles for chemotherapy and magnetic resonance imaging in liver cancer. *Biomaterials*. 2010;31(18):4995–5006. doi:10.1016/j.biomaterials.2010.02.068
68. Xu X, Zhou X, Xiao B, et al. Glutathione-responsive magnetic nanoparticles for highly sensitive diagnosis of liver metastases. *Nano Lett*. 2021;21(5):2199–2206. doi:10.1021/acs.nanolett.0c04967
69. Eftekhari A, Arjmand A, Asheghvatan A, et al. The potential application of magnetic nanoparticles for liver fibrosis theranostics. *Front Chem*. 2021;9:674786. doi:10.3389/fchem.2021.674786
70. Saraswathy A, Nazeer SS, Jeevan M, et al. Citrate coated iron oxide nanoparticles with enhanced relaxivity for in vivo magnetic resonance imaging of liver fibrosis. *Colloids Surf B Biointerfaces*. 2014;117:216–224. doi:10.1016/j.colsurfb.2014.02.034
71. Zhang YN, Poon W, Tavares AJ, McGilvray ID, Chan WCW. Nanoparticle–liver interactions: cellular uptake and hepatobiliary elimination. *J Controlled Release*. 2016;240:332–348. doi:10.1016/j.jconrel.2016.01.020
72. Nigam Y, Knight J. The lymphatic system 2: structure and function of the lymphoid organs. *Nursing Times*. 2020;116(11):44–48.
73. Pivkin IV, Peng Z, Karniadakis GE, Buffet PA, Dao M, Suresh S. Biomechanics of red blood cells in human spleen and consequences for physiology and disease. *Proc Natl Acad Sci*. 2016;113(28):7804–7809. doi:10.1073/pnas.1606751113
74. Kopeć-Szlęzak J. Macrophages and their function in hematopoietic system. *J Transfus Med*. 2014;7(3):84–92.
75. Demoy M, Andreux J, Weingarten C, Gouritin B, Guilloux V, Couvreur P. Spleen capture of nanoparticles: influence on animal species and surface characteristics. *Pharm Res*. 1999;16(1):37–41. doi:10.1023/A:1018858409737
76. Arami H, Khandhar AP, Tomitaka A, et al. In vivo multimodal magnetic particle imaging (MPI) with tailored magneto/optical contrast agents. *Biomaterials*. 2015;52:251–261. doi:10.1016/j.biomaterials.2015.02.040
77. Vu-Quang H, Yoo MK, Jeong HJ, et al. Targeted delivery of mannan-coated superparamagnetic iron oxide nanoparticles to antigen-presenting cells for magnetic resonance-based diagnosis of metastatic lymph nodes in vivo. *Acta Biomater*. 2011;7(11):3935–3945. doi:10.1016/j.actbio.2011.06.044
78. Harisinghani MG, Barentsz J, Hahn PF, et al. Noninvasive detection of clinically occult lymph-node metastases in prostate cancer. *N Engl J Med*. 2003;348(25):2491–2499. doi:10.1056/NEJMoa022749
79. Corot C, Robert P, Idee J, Port M. Recent advances in iron oxide nanocrystal technology for medical imaging☆. *Adv Drug Deliv Rev*. 2006;58(14):1471–1504. doi:10.1016/j.addr.2006.09.013
80. Hauser PV, Chang HM, Yanagawa N, Nanotechnology HM. Nanomedicine, and the Kidney. *Appl Sci*. 2021;11(16):7187. doi:10.3390/app11167187
81. Wook KJ, Cheong J, Cheong H, et al. Iron oxide-coated dextran nanoparticles with efficient renal clearance for musculoskeletal magnetic resonance imaging. *ACS Appl Nano Mater*. 2021;4(12):12943–12948. doi:10.1021/acsanm.1c03470
82. Bruners P, Braunschweig T, Hodenius M, et al. Thermoablation of malignant kidney tumors using magnetic nanoparticles: an in vivo feasibility study in a rabbit model. *Cardiovasc Intervent Radiol*. 2010;33(1):127–134. doi:10.1007/s00270-009-9583-x
83. Zuckerman JE, Choi CHJ, Han H, Davis ME. Polycation-siRNA nanoparticles can disassemble at the kidney glomerular basement membrane. *Proc Natl Acad Sci*. 2012;109(8):3137–3142. doi:10.1073/pnas.1200718109
84. Salimi M, Sarkar S, Fathi S, et al. Biodistribution, pharmacokinetics, and toxicity of dendrimer-coated iron oxide nanoparticles in BALB/c mice. *Int J Nanomedicine*. 2018;13:1483–1493. doi:10.2147/IJN.S157293
85. Zabel M. *Histology: A Textbook for Students in Medicine and Dentistry*. Edra Urban & Partner; 2021.
86. Katsnelson B, Privalova LI, Kuzmin SV, et al. Some Peculiarities of Pulmonary Clearance Mechanisms in Rats after Intratracheal Instillation of Magnetite (Fe_3 O_4) Suspensions with Different Particle Sizes in the Nanometer and Micrometer Ranges: are We Defenseless against Nanoparticles? *Int J Occup Environ Health*. 2010;16(4):508–524. doi:10.1179/oeh.2010.16.4.508
87. Katsnelson B, Privalova L, Sutunkova M, et al. Some inferences from in vivo experiments with metal and metal oxide nanoparticles: the pulmonary phagocytosis response, subchronic systemic toxicity and genotoxicity, regulatory proposals, searching for bioprotectors (a self-overview). *Int J Nanomedicine*. 2015:3013. doi:10.2147/IJN.S80843

88. Edge D, Shortt CM, Gobbo OL, et al. Pharmacokinetics and bio-distribution of novel super paramagnetic iron oxide nanoparticles (SPIONs) in the anaesthetized pig. *Clin Exp Pharmacol Physiol*. 2016;43(3):319–326. doi:10.1111/1440-1681.12533
89. Kulkarni P, Rajadurai M, Sevilimedu A, et al. Magnetic nanoparticle formulation for targeted delivery of chemotherapeutic irinotecan to lungs. *Drug Deliv Transl Res*. 2018;8(5):1450–1459. doi:10.1007/s13346-018-0527-3
90. Haeger SM, Yang Y, Schmidt EP. Heparan Sulfate in the developing, healthy, and injured lung. *Am J Respir Cell Mol Biol*. 2016;55(1):5–11. doi:10.1165/rcmb.2016-0043TR
91. Rastogi A, Yadav K, Mishra A, et al. Early diagnosis of lung cancer using magnetic nanoparticles-integrated systems. *Nanotechnol Rev*. 2022;11 (1):544–574. doi:10.1515/ntrev-2022-0032
92. Tan M, Reyes-Ortega F, Schneider-Futschik EK. Successes and challenges: inhaled treatment approaches using magnetic nanoparticles in cystic fibrosis. *Magnetochemistry*. 2020;6(2):25. doi:10.3390/magnetochemistry6020025
93. Chen M, Li X, Wang S, Yu L, Tang J, Zhou S. The role of cardiac macrophage and cytokines on ventricular arrhythmias. *Front Physiol*. 2020;11:1113. doi:10.3389/fphys.2020.01113
94. Lai RC, Arslan F, Lee MM, et al. Exosome secreted by MSC reduces myocardial ischemia/reperfusion injury. *Stem Cell Res*. 2010;4 (3):214–222. doi:10.1016/j.scr.2009.12.003
95. Bian S, Zhang L, Duan L, Wang X, Min Y, Yu H. Extracellular vesicles derived from human bone marrow mesenchymal stem cells promote angiogenesis in a rat myocardial infarction model. *J Mol Med*. 2014;92(4):387–397. doi:10.1007/s00109-013-1110-5
96. Teng X, Chen L, Chen W, Yang J, Yang Z, Shen Z. Mesenchymal stem cell-derived exosomes improve the microenvironment of infarcted myocardium contributing to angiogenesis and anti-inflammation. *Cell Physiol Biochem*. 2015;37(6):2415–2424. doi:10.1159/000438594
97. Lee JR, Park BW, Kim J, et al. Nanovesicles derived from iron oxide nanoparticles–incorporated mesenchymal stem cells for cardiac repair. *Sci Adv*. 2020;6(18):eaaz0952. doi:10.1126/sciadv.aaz0952
98. Zheng B, von See MP, Yu E, et al. Quantitative magnetic particle imaging monitors the transplantation, biodistribution, and clearance of stem cells in vivo. *Theranostics*. 2016;6(3):291–301. doi:10.7150/thno.13728
99. Huang BR, Chen PY, Huang CY, et al. Bioavailability of magnetic nanoparticles to the brain. *J Magn Magn Mater*. 2009;321(10):1604–1609. doi:10.1016/j.jmmm.2009.02.095
100. Bagchi S, Lahooti B, Chhibber T, et al. In vitro models of central nervous system barriers for blood-brain barrier permeation studies. In: Morales JO, Gaillard PJ, editors. *Nanomedicines for Brain Drug Delivery*. Vol. 157. Neuromethods. Springer US; 2021:235–253. doi:10.1007/978-1-0716-0838-8_9
101. Cecchelli R, Berezowski V, Lundquist S, et al. Modelling of the blood–brain barrier in drug discovery and development. *Nat Rev Drug Discov*. 2007;6(8):650–661. doi:10.1038/nrd2368
102. Cardoso FL, Brites D, Brito MA. Looking at the blood–brain barrier: molecular anatomy and possible investigation approaches. *Brain Res Rev*. 2010;64(2):328–363. doi:10.1016/j.brainresrev.2010.05.003
103. El Khoury J. The blood-brain barrier and pathogens: hadrian's Wall or a Dardanian gate? *Virulence*. 2012;3(2):157–158. doi:10.4161/viru.19751
104. Kaur IP, Bhandari R, Bhandari S, Kakkar V. Potential of solid lipid nanoparticles in brain targeting. *J Controlled Release*. 2008;127(2):97–109. doi:10.1016/j.jconrel.2007.12.018
105. Kreuter J, Shamenkov D, Petrov V, et al. Apolipoprotein-mediated Transport of Nanoparticle-bound Drugs Across the Blood-Brain Barrier. *J Drug Target*. 2002;10(4):317–325. doi:10.1080/10611860290031877
106. Ulbrich K, Hekmatara T, Herbert E, Kreuter J. Transferrin- and transferrin-receptor-antibody-modified nanoparticles enable drug delivery across the blood–brain barrier (BBB). *Eur J Pharm Biopharm*. 2009;71(2):251–256. doi:10.1016/j.ejpb.2008.08.021
107. Yan F, Wang Y, He S, Ku S, Gu W, Ye L. Transferrin-conjugated, fluorescein-loaded magnetic nanoparticles for targeted delivery across the blood–brain barrier. *J Mater Sci Mater Med*. 2013;24(10):2371–2379. doi:10.1007/s10856-013-4993-3
108. Akhtari M, Bragin A, Cohen M, et al. Functionalized magnetonanoparticles for MRI diagnosis and localization in epilepsy. *Epilepsia*. 2008;49 (8):1419–1430. doi:10.1111/j.1528-1167.2008.01615.x
109. Veiseh O, Sun C, Fang C, et al. Specific targeting of brain tumors with an optical/magnetic resonance imaging nanoprobe across the blood-brain barrier. *Cancer Res*. 2009;69(15):6200–6207. doi:10.1158/0008-5472.CAN-09-1157
110. Nadeem M, Ahmad M, Saeed MA, et al. Uptake and clearance analysis of Technetium ^{99m} labelled iron oxide nanoparticles in a rabbit brain. *IET Nanobiotechnol*. 2015;9(3):136–141. doi:10.1049/iet-nbt.2014.0012
111. Raut SL, Kirthivasan B, Bommana MM, Squillante E, Sadoqi M. The formulation, characterization and in vivo evaluation of a magnetic carrier for brain delivery of NIR dye. *Nanotechnology*. 2010;21(39):395102. doi:10.1088/0957-4484/21/39/395102
112. Chen R, Romero G, Christiansen MG, Mohr A, Anikeeva P. Wireless magnetothermal deep brain stimulation. *Science*. 2015;347 (6229):1477–1480. doi:10.1126/science.1261821
113. Wojtukiewicz MZ, Sierko E. The approach to antiangiogenic therapy in cancer patients. *Onkol W Prakt Klin*. 2009;5(A):A1–A14.
114. Dvorak HF, Brown LF, Detmar M, Dvorak AM. Vascular permeability factor/vascular endothelial growth factor, microvascular hyperpermeability, and angiogenesis. *Am J Pathol*. 1995;146(5):1029–1039.
115. Jain RK, Stylianopoulos T. Delivering nanomedicine to solid tumors. *Nat Rev Clin Oncol*. 2010;7(11):653–664. doi:10.1038/nrclinonc.2010.139
116. Briley-Saebo KC, Mani V, Hyafil F, Cornily JC, Fayad ZA. Fractionated feridex and positive contrast: in vivo MR imaging of atherosclerosis. *Magn Reson Med*. 2008;59(4):721–730. doi:10.1002/mrm.21541
117. Gupta AK, Wells S. Surface-modified superparamagnetic nanoparticles for drug delivery: preparation, characterization, and cytotoxicity studies. *IEEE Trans Nanobioscience*. 2004;3(1):66–73. doi:10.1109/TNB.2003.820277
118. Plank C. Silence the target. *Nat Nanotechnol*. 2009;4(9):544–545. doi:10.1038/nnano.2009.251
119. Wu X, Yu G, Lindner D, Brady-Kalnay SM, Zhang Q, Lu ZR. Peptide targeted high-resolution molecular imaging of prostate cancer with MRI. *Am J Nucl Med Mol Imaging*. 2014;4(6):525–536.
120. Jaiswal MK, Gogoi M, Dev Sarma H, Banerjee R, Bahadur D. Biocompatibility, biodistribution and efficacy of magnetic nanohydrogels in inhibiting growth of tumors in experimental mice models. *Biomater Sci*. 2014;2(3):370–380. doi:10.1039/C3BM60225G
121. Jie LY, Cai LL, Wang LJ, et al. Actively-targeted LTVSPWY peptide-modified magnetic nanoparticles for tumor imaging. *Int J Nanomedicine*. 2012;7:3981–3989. doi:10.2147/IJN.S33593

122. Krukemeyer MG, Krenn V, Jakobs M, Wagner W. Mitoxantrone-iron oxide biodistribution in blood, tumor, spleen, and liver—magnetic nanoparticles in cancer treatment. *J Surg Res*. 2012;175(1):35–43. doi:10.1016/j.jss.2011.01.060
123. Nowak-Jary J, Machnicka B. Pharmacokinetics of magnetic iron oxide nanoparticles for medical applications. *J Nanobiotechnology*. 2022;20(1):305. doi:10.1186/s12951-022-01510-w
124. Almeida JPM, Chen AL, Foster A, Drezek R. In vivo biodistribution of nanoparticles. *Nanomed*. 2011;6(5):815–835. doi:10.2217/nnm.11.79
125. Feng Q, Liu Y, Huang J, Chen K, Huang J, Xiao K. Uptake, distribution, clearance, and toxicity of iron oxide nanoparticles with different sizes and coatings. *Sci Rep*. 2018;8(1):2082. doi:10.1038/s41598-018-19628-z
126. Ashizawa K. Nanosize Particle Analysis by Dynamic Light Scattering (DLS). *YAKUGAKU ZASSHI*. 2019;139(2):237–248. doi:10.1248/yakushi.18-00171-1
127. Alexis F, Pridgen E, Molnar LK, Farokhzad OC. Factors Affecting the Clearance and Biodistribution of Polymeric Nanoparticles. *Mol Pharm*. 2008;5(4):505–515. doi:10.1021/mp800051m
128. Bourrinet P, Bengele HH, Bonnemain B, et al. Preclinical safety and pharmacokinetic profile of ferumoxtran-10, an ultrasmall superparamagnetic iron oxide magnetic resonance contrast agent. *Invest Radiol*. 2006;41(3):313–324. doi:10.1097/01.rli.0000197669.80475.dd
129. Reimer P, Tombach B. Hepatic MRI with SPIO: detection and characterization of focal liver lesions. *Eur Radiol*. 1998;8(7):1198–1204. doi:10.1007/s003300050535
130. Daldrup-Link HE. Ten Things You Might Not Know about Iron Oxide Nanoparticles. *Radiology*. 2017;284(3):616–629. doi:10.1148/radiol.2017162759
131. Harisinghani MG, Saksena MA, Hahn PF, et al. Ferumoxtran-10-enhanced MR lymphangiography: does contrast-enhanced imaging alone suffice for accurate lymph node characterization? *Am J Roentgenol*. 2006;186(1):144–148. doi:10.2214/AJR.04.1287
132. Weissleder R, Stark D, Engelstad B, et al. Superparamagnetic iron oxide: pharmacokinetics and toxicity. *Am J Roentgenol*. 1989;152(1):167–173. doi:10.2214/ajr.152.1.167
133. Chouly C, Pouliquen D, Lucet I, Jeune JJ, Jallet P. Development of superparamagnetic nanoparticles for MRI: effect of particle size, charge and surface nature on biodistribution. *J Microencapsul*. 1996;13(3):245–255. doi:10.3109/02652049609026013
134. Shao D, Meng LM, wei ZY, et al. The shape effect of magnetic mesoporous silica nanoparticles on endocytosis, biocompatibility and biodistribution. *Acta Biomater*. 2017;49:531–540. doi:10.1016/j.actbio.2016.11.007
135. Petros RA, DeSimone JM. Strategies in the design of nanoparticles for therapeutic applications. *Nat Rev Drug Discov*. 2010;9(8):615–627. doi:10.1038/nrd2591
136. Arnida J-AMM, Ray A, Peterson CM, Ghandehari H, Ghandehari H. Geometry and surface characteristics of gold nanoparticles influence their biodistribution and uptake by macrophages. *Eur J Pharm Biopharm*. 2011;77(3):417–423. doi:10.1016/j.ejpb.2010.11.010
137. Beola L, Grazú V, Fernández-Afonso Y, et al. Critical parameters to improve pancreatic cancer treatment using magnetic hyperthermia: field conditions, immune response, and particle biodistribution. *ACS Appl Mater Interfaces*. 2021;13(11):12982–12996. doi:10.1021/acsami.1c02338
138. Park J-H, von Maltzahn G, Zhang L, et al. Magnetic iron oxide nanoworms for tumor targeting and imaging. *Adv Mater*. 2008;20:1630–1635. doi:10.1002/adma.200800004
139. Kommareddy S, Amiji M. Biodistribution and pharmacokinetic analysis of long-circulating thiolated gelatin nanoparticles following systemic administration in breast cancer-bearing mice. *J Pharm Sci*. 2007;96:397–407. doi:10.1002/jps.20813
140. Papisov MI, Bogdanov A, Schaffer B, et al. Colloidal magnetic resonance contrast agents: effect of particle surface on biodistribution. *J Magn Magn Mater*. 1993;122(1–3):383–386. doi:10.1016/0304-8853(93)91115-N
141. Chertok B, Cole AJ, David AE, Yang VC. Comparison of electron spin resonance spectroscopy and inductively-coupled plasma optical emission spectroscopy for biodistribution analysis of iron-oxide nanoparticles. *Mol Pharm*. 2010;7(2):375–385. doi:10.1021/mp900161h
142. Yue ZG, Wei W, Lv PP, et al. Surface Charge Affects Cellular Uptake and Intracellular Trafficking of Chitosan-Based Nanoparticles. *Biomacromolecules*. 2011;12(7):2440–2446. doi:10.1021/bm101482r
143. Sun Z, Worden M, Wroczynskyj Y, et al. Magnetic field enhanced convective diffusion of iron oxide nanoparticles in an osmotically disrupted cell culture model of the blood–brain barrier. *Int J Nanomedicine*. 2014:3013. doi:10.2147/IJN.S62260
144. Sun Z, Worden M, Worden M, et al. Characterization of cellular uptake and toxicity of aminosilane-coated iron oxide nanoparticles with different charges in central nervous system-relevant cell culture models. *Int J Nanomedicine*. 2013:961. doi:10.2147/IJN.S39048
145. On NH, Savant S, Toews M, Miller DW. Rapid and reversible enhancement of blood–brain barrier permeability using lysophosphatidic acid. *J Cereb Blood Flow Metab*. 2013;33(12):1944–1954. doi:10.1038/jcbfm.2013.154
146. Dutta D, Sundaram SK, Teeguarden JG, et al. Adsorbed proteins influence the biological activity and molecular targeting of nanomaterials. *Toxicol Sci*. 2007;100(1):303–315. doi:10.1093/toxsci/kfm217
147. Moghimi SM, Hunter AC, Murray JC. Long-circulating and target-specific nanoparticles: theory to practice. *Pharmacol Rev*. 2001;53(2):283–318.
148. Nagayama S, ichi OK, Fukuoka Y, Higaki K, Kimura T. Time-dependent changes in opsonin amount associated on nanoparticles alter their hepatic uptake characteristics. *Int J Pharm*. 2007;342(1–2):215–221. doi:10.1016/j.ijpharm.2007.04.036
149. Camner P, Lundborg M, Låstbom L, Gerde P, Gross N, Jarstrand C. Experimental and calculated parameters on particle phagocytosis by alveolar macrophages. *J Appl Physiol*. 2002;92(6):2608–2616. doi:10.1152/japplphysiol.01067.2001
150. Leroux JC, De Jaeghere F, Anner B, Doelker E, Gurny R. An investigation on the role of plasma and serum opsonins on the evternalization of biodegradable poly(D,L-lactic acid) nanoparticles by human monocytes. *Life Sci*. 1995;57(7):695–703. doi:10.1016/0024-3205(95)00321-V
151. Chen H, Wang L, Yeh J, et al. Reducing non-specific binding and uptake of nanoparticles and improving cell targeting with an antifouling PEO-b-PγMPS copolymer coating. *Biomaterials*. 2010;31(20):5397–5407. doi:10.1016/j.biomaterials.2010.03.036
152. Cole AJ, David AE, Wang J, Galbán CJ, Hill HL, Yang VC. Polyethylene glycol modified, cross-linked starch-coated iron oxide nanoparticles for enhanced magnetic tumor targeting. *Biomaterials*. 2011;32(8):2183–2193. doi:10.1016/j.biomaterials.2010.11.040
153. Larsen EKU, Nielsen T, Wittenborn T, et al. Size-Dependent Accumulation of PEGylated Silane-Coated Magnetic Iron Oxide Nanoparticles in Murine Tumors. *ACS Nano*. 2009;3(7):1947–1951. doi:10.1021/nn900330m
154. Sun C, Du K, Fang C, et al. PEG-mediated synthesis of highly dispersive multifunctional superparamagnetic nanoparticles: their physicochemical properties and function in vivo. *ACS Nano*. 2010;4(4):2402–2410. doi:10.1021/nn100190v

155. Aggarwal P, Hall JB, McLeland CB, Dobrovolskaia MA, McNeil SE. Nanoparticle interaction with plasma proteins as it relates to particle biodistribution, biocompatibility and therapeutic efficacy. *Adv Drug Deliv Rev*. 2009;61(6):428–437. doi:10.1016/j.addr.2009.03.009
156. Liu S, Chiu-Lam A, Rivera-Rodriguez A, et al. Long circulating tracer tailored for magnetic particle imaging. *Nanotheranostics*. 2021;5(3):348–361. doi:10.7150/ntno.58548
157. Jain TK, Morales MA, Sahoo SK, Leslie-Pelecky DL, Labhasetwar V. Iron oxide nanoparticles for sustained delivery of anticancer agents. *Mol Pharm*. 2005;2(3):194–205. doi:10.1021/mp0500014
158. Briley-Saebo K, Bjornerud A, Grant D, Ahlstrom H, Berg T, Kindberg GM. Hepatic cellular distribution and degradation of iron oxide nanoparticles following single intravenous injection in rats: implications for magnetic resonance imaging. *Cell Tissue Res*. 2004;316(3):315–323. doi:10.1007/s00441-004-0884-8
159. Ikeda H, Ishii A, Sano K, et al. Activatable fluorescence imaging of macrophages in atherosclerotic plaques using iron oxide nanoparticles conjugated with indocyanine green. *Atherosclerosis*. 2018;275:1–10. doi:10.1016/j.atherosclerosis.2018.05.028
160. Wang H, Mu Q, Revia R, et al. Iron oxide-carbon core-shell nanoparticles for dual-modal imaging-guided photothermal therapy. *J Controlled Release*. 2018;289:70–78. doi:10.1016/j.jconrel.2018.09.022
161. Holig P, Bach M, Volkel T, et al. Novel RGD lipopeptides for the targeting of liposomes to integrin-expressing endothelial and melanoma cells. *Protein Eng Des Sel*. 2004;17(5):433–441. doi:10.1093/protein/gzh055
162. Corti A, Curnis F, Arap W, Pasqualini R. The neovasculature homing motif NGR: more than meets the eye. *Blood*. 2008;112(7):2628–2635. doi:10.1182/blood-2008-04-150862
163. Wu T, Ding X, Su B, Soodeen-Lalloo AK, Zhang L, Shi JY. Magnetic resonance imaging of tumor angiogenesis using dual-targeting RGD10–NGR9 ultrasmall superparamagnetic iron oxide nanoparticles. *Clin Transl Oncol*. 2018;20(5):599–606. doi:10.1007/s12094-017-1753-8
164. Curnis F, Sacchi A, Gasparri A, et al. Isoaspartate-Glycine-Arginine: a New Tumor Vasculature–Targeting Motif. *Cancer Res*. 2008;68(17):7073–7082. doi:10.1158/0008-5472.CAN-08-1272
165. Zhang C, Jugold M, Woenne EC, et al. Specific Targeting of Tumor Angiogenesis by RGD-Conjugated Ultrasmall Superparamagnetic Iron Oxide Particles Using a Clinical 1.5-T Magnetic Resonance Scanner. *Cancer Res*. 2007;67(4):1555–1562. doi:10.1158/0008-5472.CAN-06-1668
166. Oostendorp M, Douma K, Hackeng TM, et al. Quantitative molecular magnetic resonance imaging of tumor angiogenesis using cNGR-labeled paramagnetic quantum dots. *Cancer Res*. 2008;68(18):7676–7683. doi:10.1158/0008-5472.CAN-08-0689
167. Kojima C, Turkbey B, Ogawa M, et al. Dendrimer-based MRI contrast agents: the effects of PEGylation on relaxivity and pharmacokinetics. *Nanomedicine Nanotechnol Biol Med*. 2011;7(6):1001–1008. doi:10.1016/j.nano.2011.03.007
168. Longmire M, Choyke P, Kobayashi H. Dendrimer-based contrast agents for molecular imaging. *Curr Top Med Chem*. 2008;8(14):1180–1186. doi:10.2174/156802608785849021
169. Al Faraj A, Shaik AP, Shaik AS. Effect of surface coating on the biocompatibility and in vivo MRI detection of iron oxide nanoparticles after intrapulmonary administration. *Nanotoxicology*. 2015;9(7):825–834. doi:10.3109/17435390.2014.980450
170. Yang P, Xu H, Zhang Z, Yang L, Kuang H, Aguilar ZP. Surface modification affect the biodistribution and toxicity characteristics of iron oxide magnetic nanoparticles in rats. *IET Nanobiotechnol*. 2018;12(5):562–568. doi:10.1049/iet-nbt.2017.0152
171. de Oliveira PN, Moussa A, Milhau N, et al. In situ synthesis of Fe_3O_4 nanoparticles coated by chito-oligosaccharides: physico-chemical characterizations and cytotoxicity evaluation for biomedical applications. *Nanotechnology*. 2020;31(17):175602. doi:10.1088/1361-6528/ab68f9
172. Demin AM, Vakhrushev AV, Mekhaev AV, Uimin MA, Krasnov VP. Modification of Fe3O4 magnetic nanoparticles with a GRGD peptide. *Russ Chem Bull*. 2021;70(3):449–456. doi:10.1007/s11172-021-3107-5
173. Yang X, Hong H, Grailer JJ, et al. cRGD-functionalized, DOX-conjugated, and 64Cu-labeled superparamagnetic iron oxide nanoparticles for targeted anticancer drug delivery and PET/MR imaging. *Biomaterials*. 2011;32(17):4151–4160. doi:10.1016/j.biomaterials.2011.02.006
174. Kang T, Jiang M, Jiang D, et al. Enhancing glioblastoma-specific penetration by functionalization of nanoparticles with an iron-mimic peptide targeting transferrin/transferrin receptor complex. *Mol Pharm*. 2015;12(8):2947–2961. doi:10.1021/acs.molpharmaceut.5b00222
175. Jiang W, Xie H, Ghoorah D, et al. Conjugation of Functionalized SPIONs with Transferrin for Targeting and Imaging Brain Glial Tumors in Rat Model. *PLoS One*. 2012;7(5):e37376. doi:10.1371/journal.pone.0037376
176. Wang X, Chang Y, Zhang D, Tian B, Yang Y, Wei F. Transferrin-conjugated drug/dye-co-encapsulated magnetic nanocarriers for active-targeting fluorescent/magnetic resonance imaging and anti-tumor effects in human brain tumor cells. *RSC Adv*. 2016;6(107):105661–105675. doi:10.1039/C6RA20903C
177. Ghadiri M, Vasheghani-Farahani E, Atyabi F, Kobarfard F, Mohamadyar-Toupkanlou F, Hosseinkhani H. Transferrin-conjugated magnetic dextran-spermine nanoparticles for targeted drug transport across blood-brain barrier. *J Biomed Mater Res A*. 2017;105(10):2851–2864. doi:10.1002/jbm.a.36145
178. Tomitaka A, Arami H, Gandhi S, Krishnan KM. Lactoferrin conjugated iron oxide nanoparticles for targeting brain glioma cells in magnetic particle imaging. *Nanoscale*. 2015;7(40):16890–16898. doi:10.1039/C5NR02831K
179. Gupta AK, Berry C, Gupta M, Curtis A. Receptor-mediated targeting of magnetic nanoparticles using insulin as a surface ligand to prevent endocytosis. *IEEE Trans Nanobioscience*. 2003;2(4):255–261. doi:10.1109/TNB.2003.820279
180. Kou G, Wang S, Cheng C, et al. Development of SM5-1-conjugated ultrasmall superparamagnetic iron oxide nanoparticles for hepatoma detection. *Biochem Biophys Res Commun*. 2008;374(2):192–197. doi:10.1016/j.bbrc.2008.06.126
181. Thomsen LB, Thomsen MS, Moos T. Targeted drug delivery to the brain using magnetic nanoparticles. *Ther Deliv*. 2015;6(10):1145–1155. doi:10.4155/tde.15.56
182. Thomsen LB, Linemann T, Birkelund S, Tarp GA, Moos T. Evaluation of targeted delivery to the brain using magnetic immunoliposomes and magnetic force. *Materials*. 2019;12(21):3576. doi:10.3390/ma12213576
183. Wathoni N, Puluhulawa LE, Joni IM, et al. Monoclonal antibody as a targeting mediator for nanoparticle targeted delivery system for lung cancer. *Drug Deliv*. 2022;29(1):2959–2970. doi:10.1080/10717544.2022.2120566
184. Boutry S, Laurent S, Elst LV, Muller RN. Specific E-selectin targeting with a superparamagnetic MRI contrast agent. *Contrast Media Mol Imaging*. 2006;1(1):15–22. doi:10.1002/cmmi.87
185. Akal ZÜ, Alpsoy L, Baykal A. Superparamagnetic iron oxide conjugated with folic acid and carboxylated quercetin for chemotherapy applications. *Ceram Int*. 2016;42(7):9065–9072. doi:10.1016/j.ceramint.2016.02.166

186. Li L, Gao F, Jiang W, et al. Folic acid-conjugated superparamagnetic iron oxide nanoparticles for tumor-targeting MR imaging. *Drug Deliv*. 2015:1–8. doi:10.3109/10717544.2015.1006404
187. Mohammed L, Gomaa HG, Ragab D, Zhu J. Magnetic nanoparticles for environmental and biomedical applications: a review. *Particuology*. 2017;30:1–14. doi:10.1016/j.partic.2016.06.001
188. Zheng S, Han J, Jin Z, et al. Dual-Tumor-Targeted Multifunctional Magnetic Hyaluronic Acid Micelles for Enhanced MR Imaging and Combined Photothermal -Chemotherapy. *Colloids Surf B*. 2018;164:424–435. doi:10.1016/j.colsurfb.2018.02.005
189. Luo Y, Gao C, Chen W, Zhou K, Xu M. Molecular Magnetic Resonance Imaging with Contrast Agents for Assessment of Inflammatory Bowel Disease: a Systematic Review. *Contrast Media Mol Imaging*. 2020;2020:4764985. doi:10.1155/2020/4764985
190. Huang J, Shu Q, Wang L, Wu H, Wang AY, Mao H. Layer-by-layer assembled milk protein coated magnetic nanoparticle enabled oral drug delivery with high stability in stomach and enzyme-responsive release in small intestine. *Biomaterials*. 2015;39:105–113. doi:10.1016/j.biomaterials.2014.10.059
191. Mohd Tamsir N, Mohd Esa N, Shafie NH, Hussein MZ, Hamzah H, Abdullah MA. The acute effects of oral administration of phytic acid-chitosan-magnetic iron oxide nanoparticles in mice. *Int J Mol Sci*. 2019;20(17):4114. doi:10.3390/ijms20174114
192. Smith CA, Simpson CA, Kim G, Carter CJ, Feldheim DL. Gastrointestinal Bioavailability of 2.0 nm Diameter Gold Nanoparticles. *ACS Nano*. 2013;7(5):3991–3996. doi:10.1021/nn305930e
193. Butterworth MD, Illum L, Davis SS. Preparation of ultrafine silica- and PEG-coated magnetite particles. *Colloids Surf Physicochem Eng Asp*. 2001;179(1):93–102. doi:10.1016/S0927-7757(00)00633-6
194. Arruebo M, Fernández-Pacheco R, Ibarra MR, Santamaría J. Magnetic nanoparticles for drug delivery. *Nano Today*. 2007;2(3):22–32. doi:10.1016/S1748-0132(07)70084-1
195. Bailey MM, Berkland CJ. Nanoparticle formulations in pulmonary drug delivery. *Med Res Rev*. 2009;29(1):196–212. doi:10.1002/med.20140
196. Reid DW, Anderson GJ, Lamont IL. Role of lung iron in determining the bacterial and host struggle in cystic fibrosis. *Am J Physiol-Lung Cell Mol Physiol*. 2009;297(5):L795–L802. doi:10.1152/ajplung.00132.2009
197. Heilig EA, Thompson KJ, Molina RM, Ivanov AR, Brain JD, Wessling-Resnick M. Manganese and iron transport across pulmonary epithelium. *Am J Physiol-Lung Cell Mol Physiol*. 2006;290(6):L1247–L1259. doi:10.1152/ajplung.00450.2005
198. Alexiou C, Schmidt A, Klein R, Hulin P, Bergemann C, Arnold W. Magnetic drug targeting: biodistribution and dependency on magnetic field strength. *J Magn Magn Mater*. 2002;252:363–366. doi:10.1016/S0304-8853(02)00605-4
199. Wu T, Hua MY, ping CJ, et al. Effects of external magnetic field on biodistribution of nanoparticles: a histological study. *J Magn Magn Mater*. 2007;311(1):372–375. doi:10.1016/j.jmmm.2006.10.1202
200. Gutierrez L, Mejias R, Lazaro FJ, Serna CJ, Barber DF, Morales MP. Effect of anesthesia on magnetic nanoparticle biodistribution after intravenous injection. *IEEE Trans Magn*. 2013;49(1):398–401. doi:10.1109/TMAG.2012.2221162
201. Du B, Yu M, Zheng J. Transport and interactions of nanoparticles in the kidneys. *Nat Rev Mater*. 2018;3(10):358–374. doi:10.1038/s41578-018-0038-3
202. Hall JE. *Guyton and Hall Textbook of Medical Physiology*. 14th ed. Elsevier; 2020.
203. Crichton RR, Charloteaux-Wauters M. Iron transport and storage. *Eur J Biochem*. 1987;164(3):485–506. doi:10.1111/j.1432-1033.1987.tb11155.x
204. Alphandéry E, Faure S, Seksek O, Guyot F, Chebbi I. Chains of Magnetosomes Extracted from AMB-1 Magnetotactic Bacteria for Application in Alternative Magnetic Field Cancer Therapy. *ACS Nano*. 2011;5(8):6279–6296. doi:10.1021/nn201290k
205. Arbab AS, Wilson LB, Ashari P, Jordan EK, Lewis BK, Frank JA. A model of lysosomal metabolism of dextran coated superparamagnetic iron oxide (SPIO) nanoparticles: implications for cellular magnetic resonance imaging. *NMR Biomed*. 2005;18(6):383–389. doi:10.1002/nbm.970
206. Wahajuddin A. Superparamagnetic iron oxide nanoparticles: magnetic nanoplatforms as drug carriers. *Int J Nanomedicine*. 2012;3445. doi:10.2147/IJN.S30320
207. Lartigue L, Alloyeau D, Kolosnjaj-Tabi J, et al. Biodegradation of iron oxide nanocubes: high-resolution in situ monitoring. *ACS Nano*. 2013;7(5):3939–3952. doi:10.1021/nn305719y
208. Lunov O, Syrovets T, Röcker C, et al. Lysosomal degradation of the carboxydextran shell of coated superparamagnetic iron oxide nanoparticles and the fate of professional phagocytes. *Biomaterials*. 2010;31(34):9015–9022. doi:10.1016/j.biomaterials.2010.08.003
209. Arami H, Krishnan KM. Intracellular performance of tailored nanoparticle tracers in magnetic particle imaging. *J Appl Phys*. 2014;115(17):17B306. doi:10.1063/1.4867756
210. Okon E, Pouliquen D, Okon P, et al. Biodegradation of magnetite dextran nanoparticles in the rat. A histologic and biophysical study. *Lab Investig J Tech Methods Pathol*. 1994;71(6):895–903.
211. Zhang X, Liu C, Yuan Y, Shan X, Sheng Y, Xu F. Reduction and suppression of methemoglobin loaded in the polymeric nanoparticles intended for blood substitutes. *J Biomed Mater Res B Appl Biomater*. 2008;87B(2):354–363. doi:10.1002/jbm.b.31110
212. Jensen JH, Tang H, Tosti CL, et al. Separate MRI quantification of dispersed (ferritin-like) and aggregated (hemosiderin-like) storage iron. *Magn Reson Med*. 2010;63(5):1201–1209. doi:10.1002/mrm.22273
213. Nosrati H, Tarantash M, Bochani S, et al. Glutathione (GSH) Peptide Conjugated Magnetic Nanoparticles As Blood–Brain Barrier Shuttle for MRI-Monitored Brain Delivery of Paclitaxel. *ACS Biomater Sci Eng*. 2019;5(4):1677–1685. doi:10.1021/acsbiomaterials.8b01420
214. Gu X, Song Q, Zhang Q, et al. Clearance of two organic nanoparticles from the brain via the paravascular pathway. *J Controlled Release*. 2020;322:31–41. doi:10.1016/j.jconrel.2020.03.009
215. Arms L, Smith DW, Flynn J, et al. Advantages and limitations of current techniques for analyzing the biodistribution of nanoparticles. *Front Pharmacol*. 2018;9:802. doi:10.3389/fphar.2018.00802
216. Pham B, Colvin E, Pham N, et al. Biodistribution and clearance of stable superparamagnetic maghemite iron oxide nanoparticles in mice following intraperitoneal administration. *Int J Mol Sci*. 2018;19(1):205. doi:10.3390/ijms19010205
217. Robson AL, Dastoor PC, Flynn J, et al. Advantages and limitations of current imaging techniques for characterizing liposome morphology. *Front Pharmacol*. 2018;9:80. doi:10.3389/fphar.2018.00080
218. Shigematsu A, Motoji N, Hatori A, Satoh T. Progressive application of autoradiography in pharmacokinetic and metabolic studies for the development of new drugs. *Regul Toxicol Pharmacol*. 1995;22(2):122–142. doi:10.1006/rtph.1995.1078

219. Mayhew TM, Mühlfeld C, Vanhecke D, Ochs M. A review of recent methods for efficiently quantifying immunogold and other nanoparticles using TEM sections through cells, tissues and organs. *Ann Anat - Anat Anz*. 2009;191(2):153–170. doi:10.1016/j.aanat.2008.11.001
220. García-Negrete CA, Jiménez de Haro MC, Blasco J, Soto M, Fernández A. STEM-in-SEM high resolution imaging of gold nanoparticles and bivalve tissues in bioaccumulation experiments. *Analyst*. 2015;140(9):3082–3089. doi:10.1039/C4AN01643B
221. Mühlfeld C, Rothen-Rutishauser B, Vanhecke D, Blank F, Gehr P, Ochs M. Visualization and quantitative analysis of nanoparticles in the respiratory tract by transmission electron microscopy. *Part Fibre Toxicol*. 2007;4(1):11. doi:10.1186/1743-8977-4-11
222. Jong WHD, Burger MC, Verheijen MA, Geertsma RE. Detection of the presence of gold nanoparticles in organs by transmission electron microscopy. *Materials*. 2010;3(9):4681–4694. doi:10.3390/ma3094681
223. Kempen PJ, Thakor AS, Zavaleta C, Gambhir SS, Sinclair R. A scanning transmission electron microscopy approach to analyzing large volumes of tissue to detect nanoparticles. *Microsc Microanal*. 2013;19(5):1290–1297. doi:10.1017/S143192761300192X
224. Paddock SW. Principles and practices of laser scanning confocal microscopy. *Mol Biotechnol*. 2000;16(2):127–150. doi:10.1385/MB:16:2:127
225. Huang Y, Mao K, Zhang B, Zhao Y. Superparamagnetic iron oxide nanoparticles conjugated with folic acid for dual target-specific drug delivery and MRI in cancer theranostics. *Mater Sci Eng C*. 2017;70:763–771. doi:10.1016/j.msec.2016.09.052
226. Strijkers GJ, Mulder WJ, van Tilborg GA, Nicolay K. MRI contrast agents: current status and future perspectives. *Anticancer Agents Med Chem*. 2007;7(3):291–305. doi:10.2174/187152007780618135
227. Kamaly N, Miller AD. Paramagnetic liposome nanoparticles for cellular and tumour imaging. *Int J Mol Sci*. 2010;11(4):1759–1776. doi:10.3390/ijms11041759
228. Kim BH, Lee N, Kim H, et al. Large-Scale Synthesis of Uniform and Extremely Small-Sized Iron Oxide Nanoparticles for High-Resolution T_1 Magnetic Resonance Imaging Contrast Agents. *J Am Chem Soc*. 2011;133(32):12624–12631. doi:10.1021/ja203340u
229. Pablico-Lansigan MH, Situ SF, Samia ACS. Magnetic particle imaging: advancements and perspectives for real-time in vivo monitoring and image-guided therapy. *Nanoscale*. 2013;5(10):4040. doi:10.1039/c3nr00544e
230. Ferguson RM, Minard KR, Krishnan KM. Optimization of nanoparticle core size for magnetic particle imaging. *J Magn Magn Mater*. 2009;321(10):1548–1551. doi:10.1016/j.jmmm.2009.02.083
231. Gleich B, Weizenecker J. Tomographic imaging using the nonlinear response of magnetic particles. *Nature*. 2005;435(7046):1214–1217. doi:10.1038/nature03808
232. Gleich B, Weizenecker J, Borgert J. Experimental results on fast 2D-encoded magnetic particle imaging. *Phys Med Biol*. 2008;53(6):N81–N84. doi:10.1088/0031-9155/53/6/N01
233. Madru R, Kjellman P, Olsson F, et al. ^{99m} Tc-Labeled Superparamagnetic Iron Oxide Nanoparticles for Multimodality SPECT/MRI of Sentinel Lymph Nodes. *J Nucl Med*. 2012;53(3):459–463. doi:10.2967/jnumed.111.092437
234. Pimlott SL, Sutherland A. Molecular tracers for the PET and SPECT imaging of disease. *Chem Soc Rev*. 2011;40(1):149–162. doi:10.1039/B922628C
235. Van Audenhaege K, Van Holen R, Vandenberghe S, Vanhove C, Metzler SD, Moore SC. Review of SPECT collimator selection, optimization, and fabrication for clinical and preclinical imaging: review of SPECT collimator selection, optimization, and fabrication. *Med Phys*. 2015;42(8):4796–4813. doi:10.1118/1.4927061
236. Hong Y, Zhu H, Hu J, et al. Synthesis and radiolabeling of 111In-core-cross linked polymeric micelle-octreotide for near-infrared fluoroscopy and single photon emission computed tomography imaging. *Bioorg Med Chem Lett*. 2014;24(12):2781–2785. doi:10.1016/j.bmcl.2014.03.050
237. Wiekhorst F, Steinhoff U, Eberbeck D, Trahms L. Magnetorelaxometry assisting biomedical applications of magnetic nanoparticles. *Pharm Res*. 2012;29(5):1189–1202. doi:10.1007/s11095-011-0630-3
238. Dames P, Gleich B, Flemmer A, et al. Targeted delivery of magnetic aerosol droplets to the lung. *Nat Nanotechnol*. 2007;2(8):495–499. doi:10.1038/nnano.2007.217
239. Johnson C, Adolphi NL, Butler KL, et al. Magnetic relaxometry with an atomic magnetometer and SQUID sensors on targeted cancer cells. *J Magn Magn Mater*. 2012;324(17):2613–2619. doi:10.1016/j.jmmm.2012.03.015
240. Kötitz R, Weitschies W, Trahms L, Semmler W. Investigation of Brownian and Néel relaxation in magnetic fluids. *J Magn Magn Mater*. 1999;201(1–3):102–104. doi:10.1016/S0304-8853(99)00065-7
241. Roessler MM, Salvadori E. Principles and applications of EPR spectroscopy in the chemical sciences. *Chem Soc Rev*. 2018;47(8):2534–2553. doi:10.1039/C6CS00565A
242. Gamarra LF, Pontuschka WM, Amaro E, et al. Kinetics of elimination and distribution in blood and liver of biocompatible ferrofluids based on Fe3O4 nanoparticles: an EPR and XRF study. *Mater Sci Eng C*. 2008;28(4):519–525. doi:10.1016/j.msec.2007.06.005
243. Ślawska-Waniewska A, Mosiniewicz-Szablewska E, Nedelko N, Gałązka-Friedman J, Friedman A. Magnetic studies of iron-entities in human tissues. *J Magn Magn Mater*. 2004;272-276:2417–2419. doi:10.1016/j.jmmm.2003.12.843
244. Danhier P, Gallez B. Electron paramagnetic resonance: a powerful tool to support magnetic resonance imaging research: EPR AS A TOOL TO SUPPORT MRI RESEARCH. *Contrast Media Mol Imaging*. 2015;10(4):266–281. doi:10.1002/cmmi.1630
245. Gobbo OL, Wetterling F, Vaes P, et al. Biodistribution and pharmacokinetic studies of SPION using particle electron paramagnetic resonance, MRI and ICP-MS. *Nanomed*. 2015;10(11):1751–1760. doi:10.2217/nnm.15.22
246. Zettner A. Principles and Applications of Atomic Absorption Spectroscopy. *Adv Clin Chem*. 1964;7:1–62. doi:10.1016/S0065-2423(08)60372-8
247. Van Loon JC. *Analytical Atomic Absorption Spectroscopy: Selected Methods*. Academic Press; 1980.
248. Szczepaniak W. *Metody instrumentalne w analizie chemicznej*. Naukowe PWN; 2002.
249. Welz B. *Atomic Absorption Spectrometry*. 3rd ed. Wiley-VCH; 1999.
250. Ficko BW, Nadar PM, Hoopes PJ, Diamond SG. Development of a magnetic nanoparticle susceptibility magnitude imaging array. *Phys Med Biol*. 2014;59(4):1047–1071. doi:10.1088/0031-9155/59/4/1047
251. Park K, Harrah T, Goldberg EB, Guertin RP, Sonkusale S. Multiplexed sensing based on Brownian relaxation of magnetic nanoparticles using a compact AC susceptometer. *Nanotechnology*. 2011;22(8):085501. doi:10.1088/0957-4484/22/8/085501

252. Narayanasamy KK, Cruz-Acuña M, Rinaldi C, Everett J, Dobson J, Telling ND. Alternating current (AC) susceptibility as a particle-focused probe of coating and clustering behaviour in magnetic nanoparticle suspensions. *J Colloid Interface Sci*. 2018;532:536–545. doi:10.1016/j.jcis.2018.08.014
253. Gutiérrez L, Romero S, da Silva GB, et al. Degradation of magnetic nanoparticles mimicking lysosomal conditions followed by AC susceptibility. *Biomed Eng Biomed Tech*. 2015;60(5). doi:10.1515/bmt-2015-0043
254. Costo R, Heinke D, Grüttner C, et al. Improving the reliability of the iron concentration quantification for iron oxide nanoparticle suspensions: a two-institutions study. *Anal Bioanal Chem*. 2019;411(9):1895–1903. doi:10.1007/s00216-018-1463-2
255. Albanese A, Tsoi KM, Chan WCW. Simultaneous quantification of cells and nanomaterials by inductive-coupled plasma techniques. *J Lab Autom*. 2013;18(1):99–104. doi:10.1177/2211068212457039
256. Kruszewska J, Sikorski J, Samsonowicz-Górski J, Matczuk M. A CE-ICP-MS/MS method for the determination of superparamagnetic iron oxide nanoparticles under simulated physiological conditions. *Anal Bioanal Chem*. 2020;412(29):8145–8153. doi:10.1007/s00216-020-02948-3
257. Kuznetsova OV, Mokhodoeva OB, Maksimova VV, et al. High-resolution ICP-MS approach for characterization of magnetic nanoparticles for biomedical applications. *J Pharm Biomed Anal*. 2020;189:113479. doi:10.1016/j.jpba.2020.113479